Supplementary Information: Spreading, pinching, and coalescence: the Ohnesorge units

M.A. Fardin,[1,2,*] M. Hautefeuille,[2,3,4] and V. Sharma[1,5]

[1] *The Academy of Bradylogists*
[2] *Université de Paris, CNRS, Institut Jacques Monod, F-75006 Paris, France*
[3] *Facultad de Ciencias, Departamento de Fisica, Universidad Nacional Autónoma de México,Ciudad Universitaria, DF 04510, Mexico*
[4] *Institut de Biologie Paris Seine, Sorbonne Université, 7 quai Saint Bernard, 75005 Paris, France*
[5] *Department of Chemical Engineering, University of Illinois at Chicago, Chicago, Illinois 60608, UnitedStates*

(Dated: March 24, 2022)

Contents

*Corresponding author ; Electronic address: marc-antoine.fardin@ijm.fr

Label	Type	Symbol	Reference
Cazabat1986	Spreading	♦	A. Cazabat and M. C. Stuart, *J. Phys. Chem.* **90**, 5845 (1986)
Biance2004	Spreading	●	A.-L. Biance *et al.*, *Phys. Rev. E* **69**, 016301 (2004)
Eddi2013	Spreading	■	A. Eddi *et al.*, *Phys. Fluids* **25**, 013102 (2013)
Chen2014	Spreading	⬢	L. Chen and E. Bonaccurso, *Phys. Rev. E* **90**, 022401 (2014)
Menchaca2001	Coalescence	▽	A. Menchaca-Rocha *et al.*, *Phys. Rev. E* **63**, 046309 (2001)
Wu2004	Coalescence	⬠	M. Wu *et al.*, *Phys. Fluids* **16**, L51–L54 (2004)
Yao2005	Coalescence	▷	W. Yao *et al.*, *Phys. Rev. E* **71**, 016309 (2005)
Thoroddsen2005	Coalescence	⬡	S.T. Thoroddsen *et al.*, *J. Fluid Mech.* **527**, 85–114 (2005)
Thoroddsen2005b	Coalescence	⬡	S.T. Thoroddsen *et al.*, *Phys. Fluids* **17**, 071703 (2005)
Aarts2005	Coalescence	□	D. Aarts *et al.*, *Phys. Rev. Lett.* **95**, 164503 (2005)
Aarts2008	Coalescence	□	D. Aarts and H. Lekkerkerker, *J. Fluid Mech.* **71**, 275–294 (2008)
Yokota2011	Coalescence	⬡	M. Yokota and K. Okumura, *PNAS* **108**, 6395–6398 (2011)
Paulsen2011	Coalescence	○	J. Paulsen *et al.*, *Phys. Rev. Lett.* **106**, 114501 (2011)
Paulsen2014	Coalescence	○	J. Paulsen *et al.*, *Nat. Commun.* **5**, 1–7 (2014)
Soto2018	Coalescence	△	A.M. Soto *et al.*, *J. Fluid Mech.* **846**, 143–165 (2018)
Rahman2019	Coalescence	◇	M. Rahman *et al.*, *Phys. Fluids* **31**, 012104 (2019)
Chen1997	Pinching	⅄	Y.J. Chen and P.H. Steen, *J. Fluid Mech.* **341**, 245–267 (1997)
McKinley2000	Pinching	≺	G.H. McKinley and A. Tripathi, *J. Rheol.* **44**, 653–670 (2000)
Chen2002	Pinching	✖	A.U. Chen *et al.*, *Phys. Rev. Lett.* **88**, 174501 (2002)
Burton2004	Pinching	⋆	J.C. Burton *et al.*, *Phys. Rev. Lett.* **92**, 244505 (2004)
Burton2005	Pinching	⋆	J.C. Burton *et al.*, *Phys. Rev. Lett.* **94**, 184502 (2005)
Burton2007	Pinching	⋆	J.C. Burton *et al.*, *Phys. Rev. E* **75**, 036311 (2007)
Keim2006	Pinching	×	N.C. Keim *et al.*, *Phys. Rev. Lett.* **97**, 144503 (2006)
Bolanos2009	Pinching	+	R. Bolanos-Jiménez *et al.*, *Phys. Fluids* **21**, 072103 (2009)
Goldstein2010	Pinching	⅄	R.E. Goldstein *et al.*, *PNAS* **107**, 21979–21984 (2010)

TABLE I: Summary of the original studies reproduced in the article.

I. EXPERIMENTAL DATA SUMMARY

Our study provides a meta-analysis of a number of experiments on spreading, coalescence and pinching of fluids of various properties. In this section we explain the protocol we followed to extract the data sets from the original articles and we give tables summarizing the properties of all experiments reproduced in the figures of the article.

A. Data extraction

All data were extracted semi-manually from the figures of the original articles given in Table I. For a given figure, the data points were identified manually on the free imagining software Fiji [1]. The coordinates of the data points were stored and converted to standard units (seconds and meters). The precision is expected to be on the order of the size of the symbols used in the original graphs. When the sampling was high and multiple data points overlapped we only selected a subsets of the original data points. We omitted data points with large error bars, which usually corresponded to the first few measurements at the limit of the resolution of the experiment. All extracted data sets (t and d) are given as two-columns text-files in the supplementary archive '**DataSets.zip**'.

B. Data summary

The values of the material parameters ρ, η and Γ, of the extrinsic size D, and the associated value of the Ohnesorge number for spreading, coalescence and pinching experiments are given in Tables II, III and IV respectively, which can be found in the supplementary file '**DataSummary.csv**'. More details on each data set are given in section VI.

C. Extended figure legends

The labels associated with each data set defined in Tables II, III and IV are used in the legends of each figure present in the supplementary archive '**FigureLegends.zip**'. For each figure of the article and of the present supplementary

Label	$\boldsymbol{\rho}$ (kg.m^{-3})	$\boldsymbol{\eta}$ (kg.m^{-1}.s^{-1})	$\boldsymbol{\Gamma}$ (kg.s^{-2})	$\boldsymbol{D}$ (m)	**Oh**	$\boldsymbol{\tau_{vi}}$ (s)	$\boldsymbol{\tau_{ic}}$ (s)	$\boldsymbol{\tau_{vc}}$ (s)	$\boldsymbol{\tau_{o}}$ (s)
Cazabat1986˙Fig1a˙0p78	9.00e+02	2.00e-02	2.00e-02	5.71e-04	1.97e-01	1.47e-02	2.89e-03	5.71e-04	2.22e-05
Cazabat1986˙Fig1a˙1p5	9.00e+02	2.00e-02	2.00e-02	7.10e-04	1.77e-01	2.27e-02	4.01e-03	7.10e-04	2.22e-05
Cazabat1986˙Fig1a˙2p9	9.00e+02	2.00e-02	2.00e-02	8.84e-04	1.59e-01	3.52e-02	5.58e-03	8.84e-04	2.22e-05
Cazabat1986˙Fig1a˙3p8	9.00e+02	2.00e-02	2.00e-02	9.68e-04	1.52e-01	4.21e-02	6.38e-03	9.68e-04	2.22e-05
Cazabat1986˙Fig1a˙4p7	9.00e+02	2.00e-02	2.00e-02	1.04e-03	1.46e-01	4.85e-02	7.10e-03	1.04e-03	2.22e-05
Cazabat1986˙Fig1a˙7p8	9.00e+02	2.00e-02	2.00e-02	1.23e-03	1.34e-01	6.80e-02	9.15e-03	1.23e-03	2.22e-05
Cazabat1986˙Fig1a˙14p4	9.00e+02	2.00e-02	2.00e-02	1.51e-03	1.21e-01	1.02e-01	1.24e-02	1.51e-03	2.22e-05
Cazabat1986˙Fig1b˙37p9	9.00e+02	1.00e+00	2.00e-02	2.08e-03	5.16e+00	3.90e-03	2.02e-02	1.04e-01	2.78e+00
Cazabat1986˙Fig1b˙5p8	9.00e+02	1.00e+00	2.00e-02	1.11e-03	7.06e+00	1.12e-03	7.89e-03	5.57e-02	2.78e+00
Cazabat1986˙Fig1b˙4p03	9.00e+02	1.00e+00	2.00e-02	9.87e-04	7.50e+00	8.76e-04	6.57e-03	4.93e-02	2.78e+00
Cazabat1986˙Fig1b˙1p35	9.00e+02	1.00e+00	2.00e-02	6.85e-04	9.00e+00	4.23e-04	3.81e-03	3.43e-02	2.78e+00
Cazabat1986˙Fig1b˙0p35	9.00e+02	1.00e+00	2.00e-02	4.37e-04	1.13e+01	1.72e-04	1.94e-03	2.18e-02	2.78e+00
Biance2004˙Fig3˙0p27	1.00e+03	1.00e-03	7.20e-02	2.70e-04	7.17e-03	7.29e-02	5.23e-04	3.75e-06	1.93e-10
Biance2004˙Fig3˙0p7	1.00e+03	1.00e-03	7.20e-02	7.00e-04	4.45e-03	4.90e-01	2.18e-03	9.72e-06	1.93e-10
Biance2004˙Fig3˙1p2	1.00e+03	1.00e-03	7.20e-02	1.20e-03	3.40e-03	1.44e+00	4.90e-03	1.67e-05	1.93e-10
Eddi2013˙Fig4˙0p37	1.20e+03	5.00e-02	6.47e-02	3.70e-04	2.95e-01	3.30e-03	9.71e-04	2.86e-04	2.48e-05
Eddi2013˙Fig4˙0p5	1.20e+03	5.00e-02	6.47e-02	5.00e-04	2.53e-01	6.02e-03	1.53e-03	3.86e-04	2.48e-05
Eddi2013˙Fig4˙0p63	1.20e+03	5.00e-02	6.47e-02	6.30e-04	2.26e-01	9.56e-03	2.16e-03	4.87e-04	2.48e-05
Eddi2013˙Fig5a˙105deg	1.20e+03	5.00e-02	6.47e-02	5.00e-04	2.53e-01	6.02e-03	1.53e-03	3.86e-04	2.48e-05
Eddi2013˙Fig5b˙0	9.98e+02	1.00e-03	7.20e-02	5.00e-04	5.28e-03	2.49e-01	1.32e-03	6.94e-06	1.93e-10
Eddi2013˙Fig5b˙115	9.98e+02	1.00e-03	7.20e-02	5.00e-04	5.28e-03	2.49e-01	1.32e-03	6.94e-06	1.93e-10
Eddi2013˙Fig6˙water	9.98e+02	1.00e-03	7.20e-02	5.00e-04	5.28e-03	2.49e-01	1.32e-03	6.94e-06	1.93e-10
Eddi2013˙Fig6˙11	1.20e+03	1.15e-02	6.73e-02	5.00e-04	5.71e-02	2.62e-02	1.50e-03	8.54e-05	2.79e-07
Eddi2013˙Fig6˙1120	1.26e+03	1.12e+00	6.31e-02	5.00e-04	5.61e+00	2.82e-04	1.58e-03	8.87e-03	2.80e-01
Eddi2013˙Fig6˙220	1.24e+03	2.20e-01	6.34e-02	5.00e-04	1.11e+00	1.41e-03	1.56e-03	1.74e-03	2.14e-03
Chen2014˙Fig3b˙60cP	1.21e+03	6.01e-02	6.23e-02	9.00e-04	2.31e-01	1.63e-02	3.76e-03	8.68e-04	4.63e-05
Chen2014˙Fig3b˙35p5cP	1.19e+03	3.55e-02	6.35e-02	9.00e-04	1.36e-01	2.73e-02	3.70e-03	5.03e-04	9.29e-06

TABLE II: Summary of the properties of all spreading experiments reproduced in the article: density ρ, viscosity η, surface tension Γ, extrinsic size D, Ohnesorge number $\mathrm{Oh} = \eta/(\rho\Gamma D)^{\frac{1}{2}}$, together with the values of the four time scales τ_{vi}, τ_{ic}, τ_{vc} and τ_o. The content of this table is available in the supplementary file '**DataSummary.csv**'.

material, the archive contain a txt file with the labels of all the data plotted in the given figure. The labels can then be used to recover the values of the material parameters, of D, and of any additional metric by using the various tables of this supplementary material.

Label	$\boldsymbol{\rho}$ (kg.m^{-3})	$\boldsymbol{\eta}$ (kg.m^{-1}.s^{-1})	$\boldsymbol{\Gamma}$ (kg.s^{-2})	$\boldsymbol{D}$ (m)	**Oh**	$\boldsymbol{\tau_{vi}}$ (s)	$\boldsymbol{\tau_{ic}}$ (s)	$\boldsymbol{\tau_{vc}}$ (s)	$\boldsymbol{\tau_{o}}$ (s)
Menchaca2001˙Fig9	1.36e+04	1.60e-03	4.35e-01	2.60e-03	4.08e-04	5.74e+01	2.34e-02	9.56e-06	1.59e-12
Wu2004˙Fig4˙1p94	9.98e+02	1.00e-03	7.27e-02	1.94e-03	2.67e-03	3.76e+00	1.00e-02	2.67e-05	1.90e-10
Yao2005˙100000cS˙5cm	9.70e+02	9.70e+01	9.00e-03	5.00e-02	1.47e+02	2.50e-02	3.67e+00	5.39e+02	1.16e+07
Yao2005˙100000cS˙0p5cm	9.70e+02	9.70e+01	9.00e-03	5.00e-03	4.64e+02	2.50e-04	1.16e-01	5.39e+01	1.16e+07
Yao2005˙10000cS˙0p5cm	9.70e+02	9.70e+00	9.00e-03	5.00e-03	4.64e+01	2.50e-03	1.16e-01	5.39e+00	1.16e+04
Yao2005˙1000cS˙0p5cm	9.70e+02	9.70e-01	9.00e-03	5.00e-03	4.64e+00	2.50e-02	1.16e-01	5.39e-01	1.16e+01
Thoroddsen2005˙Fig6	1.00e+03	1.00e-03	7.20e-02	1.12e-03	3.53e-03	1.24e+00	4.39e-03	1.55e-05	1.93e-10
Thoroddsen2005b˙Fig4	7.89e+02	1.20e-03	2.15e-02	1.30e-03	8.08e-03	1.11e+00	8.98e-03	7.26e-05	4.74e-09
Aarts2005˙Fig2˙100mPas	9.70e+02	1.00e-01	2.00e-02	2.00e-03	5.08e-01	3.88e-02	1.97e-02	1.00e-02	2.58e-03
Aarts2005˙Fig2˙1Pas	9.70e+02	1.00e+00	2.00e-02	2.00e-03	5.08e+00	3.88e-03	1.97e-02	1.00e-01	2.58e+00
Aarts2005˙Fig2˙500mPas	9.70e+02	5.00e-01	2.00e-02	2.00e-03	2.54e+00	7.76e-03	1.97e-02	5.00e-02	3.22e-01
Aarts2005˙Fig2˙300mPas	9.70e+02	3.00e-01	2.00e-02	2.00e-03	1.52e+00	1.29e-02	1.97e-02	3.00e-02	6.96e-02
Aarts2005˙Fig3˙5mPas	9.98e+02	5.00e-03	2.00e-02	2.00e-03	2.50e-02	7.98e-01	2.00e-02	5.00e-04	3.13e-07
Aarts2005˙Fig3˙20mPas	9.98e+02	2.00e-02	2.00e-02	2.00e-03	1.00e-01	2.00e-01	2.00e-02	2.00e-03	2.00e-05
Aarts2005˙Fig3˙50mPas	9.98e+02	5.00e-02	2.00e-02	2.00e-03	2.50e-01	7.98e-02	2.00e-02	5.00e-03	3.13e-04
Aarts2005˙Fig3˙1mPas	9.98e+02	1.00e-03	7.20e-02	2.00e-03	2.64e-03	3.99e+00	1.05e-02	2.78e-05	1.93e-10
Aarts2008˙Fig9˙bubb17	1.17e+03	8.00e-03	1.60e-07	1.70e-05	1.42e+02	4.23e-05	5.99e-03	8.50e-01	1.71e+04
Aarts2008˙Fig9˙drop17	1.17e+03	3.10e-02	1.60e-07	1.70e-05	5.50e+02	1.09e-05	5.99e-03	3.29e+00	9.95e+05
Yokota2011˙Fig2˙289	1.23e+03	2.89e-01	2.00e-02	1.97e-03	1.31e+00	1.66e-02	2.17e-02	2.85e-02	4.91e-02
Yokota2011˙Fig2˙888	1.26e+03	8.88e-01	2.00e-02	2.03e-03	3.92e+00	5.86e-03	2.30e-02	9.02e-02	1.39e+00
Paulsen2011˙Fig2˙1p9	1.20e+03	1.90e-03	6.50e-02	2.00e-03	4.81e-03	2.53e+00	1.22e-02	5.85e-05	1.35e-09
Paulsen2011˙Fig2˙11	1.20e+03	1.10e-02	6.50e-02	2.00e-03	2.79e-02	4.36e-01	1.22e-02	3.38e-04	2.63e-07
Paulsen2011˙Fig2˙48	1.20e+03	4.80e-02	6.50e-02	2.00e-03	1.22e-01	1.00e-01	1.22e-02	1.48e-03	2.18e-05
Paulsen2011˙Fig2˙230	1.20e+03	2.30e-01	6.50e-02	2.00e-03	5.82e-01	2.09e-02	1.22e-02	7.08e-03	2.40e-03
Paulsen2014˙Fig1	1.07e+03	1.00e-03	3.90e-02	2.00e-03	3.46e-03	4.28e+00	1.48e-02	5.13e-05	6.14e-10
Soto2018˙Fig5	1.01e+03	9.64e-04	5.87e-02	3.00e-04	7.21e-03	9.47e-02	6.83e-04	4.93e-06	2.56e-10
Rahman2019˙Fig6˙6p65	1.26e+03	1.21e+00	6.40e-02	4.22e-04	6.54e+00	1.86e-04	1.22e-03	7.96e-03	3.40e-01
Rahman2019˙Fig6˙1p84	1.24e+03	3.33e-01	6.47e-02	4.10e-04	1.84e+00	6.26e-04	1.15e-03	2.11e-03	7.11e-03
Rahman2019˙Fig6˙0p146	1.17e+03	2.50e-02	6.71e-02	3.78e-04	1.45e-01	6.68e-03	9.70e-04	1.41e-04	2.97e-06
Rahman2019˙Fig6˙0p00692	9.98e+02	1.00e-03	7.28e-02	3.64e-04	6.15e-03	1.32e-01	8.13e-04	5.00e-06	1.89e-10

TABLE III: Summary of the properties of all coalescence experiments reproduced in the article: density ρ, viscosity η, surface tension Γ, extrinsic size D, Ohnesorge number $\mathrm{Oh} = \eta/(\rho\Gamma D)^{\frac{1}{2}}$, together with the values of the four time scales τ_{vi}, τ_{ic}, τ_{vc} and τ_o. The content of this table is available in the supplementary file '**DataSummary.csv**'.

Label	$\boldsymbol{\rho}$ (kg.m^{-3})	$\boldsymbol{\eta}$ (kg.m^{-1}.s^{-1})	$\boldsymbol{\Gamma}$ (kg.s^{-2})	$\boldsymbol{D}$ (m)	**Oh**	$\boldsymbol{\tau_{vi}}$ (s)	$\boldsymbol{\tau_{ic}}$ (s)	$\boldsymbol{\tau_{vc}}$ (s)	$\boldsymbol{\tau_{o}}$ (s)
Chen1997˙Fig7	1.20e+00	3.00e-03	6.00e-02	1.90e-02	8.11e-02	1.44e-01	1.17e-02	9.50e-04	6.25e-06
McKinley2000˙Fig4	1.26e+03	1.03e+00	6.48e-02	3.00e-03	2.08e+00	1.10e-02	2.29e-02	4.77e-02	2.07e-01
Chen2002˙Fig3	9.98e+02	9.13e-04	7.06e-02	3.60e-03	1.81e-03	1.42e+01	2.57e-02	4.66e-05	1.53e-10
Burton2004˙Fig5	1.36e+04	1.50e-03	4.80e-01	3.18e-03	3.30e-04	9.13e+01	3.01e-02	9.92e-06	1.08e-12
Burton2005˙0p9	9.98e+02	9.00e-04	7.20e-02	3.20e-03	1.88e-03	1.14e+01	2.13e-02	4.00e-05	1.41e-10
Burton2005˙37p4	1.00e+03	3.74e-02	6.50e-02	3.20e-03	8.20e-02	2.74e-01	2.25e-02	1.84e-03	1.24e-05
Burton2005˙1011	1.20e+03	1.01e+00	6.30e-02	3.20e-03	2.06e+00	1.22e-02	2.50e-02	5.14e-02	2.17e-01
Burton2007˙Fig7	1.25e+02	nan	2.87e-04	5.30e-04	nan	nan	8.06e-03	nan	nan
Keim2006˙Fig2˙4p1	1.00e+03	1.00e-03	7.20e-02	4.10e-03	1.84e-03	1.68e+01	3.09e-02	5.69e-05	1.93e-10
Keim2006˙Fig2˙1p5	1.00e+03	1.00e-03	7.20e-02	1.50e-03	3.04e-03	2.25e+00	6.85e-03	2.08e-05	1.93e-10
Bolanos2009˙Fig6˙water	9.98e+02	1.00e-03	7.20e-02	4.19e-04	5.76e-03	1.75e-01	1.01e-03	5.82e-06	1.93e-10
Bolanos2009˙Fig7˙water	9.98e+02	1.00e-03	7.20e-02	1.60e-03	2.95e-03	2.55e+00	7.53e-03	2.22e-05	1.93e-10
Bolanos2009˙Fig6˙O2	9.30e+02	9.30e-03	1.99e-02	2.50e-04	1.37e-01	6.25e-03	8.55e-04	1.17e-04	2.18e-06
Bolanos2009˙Fig7˙O7	9.13e+02	4.60e-03	1.94e-02	7.50e-04	3.99e-02	1.12e-01	4.46e-03	1.78e-04	2.83e-07
Bolanos2009˙Fig7˙O8	9.30e+02	9.30e-03	1.99e-02	7.50e-04	7.89e-02	5.63e-02	4.44e-03	3.51e-04	2.18e-06
Bolanos2009˙Fig7˙O9	9.37e+02	1.87e-02	2.02e-02	7.50e-04	1.57e-01	2.82e-02	4.42e-03	6.94e-04	1.71e-05
Bolanos2009˙Fig8˙G1	1.18e+03	2.44e-02	6.69e-02	1.02e-03	8.57e-02	5.09e-02	4.36e-03	3.74e-04	2.75e-06
Bolanos2009˙Fig8˙G2	1.24e+03	2.22e-01	6.42e-02	1.02e-03	7.80e-01	5.83e-03	4.55e-03	3.55e-03	2.16e-03
Bolanos2009˙Fig8˙G4	1.25e+03	8.00e-01	6.31e-02	1.02e-03	2.81e+00	1.65e-03	4.63e-03	1.30e-02	1.03e-01
Bolanos2009˙Fig9˙G5	1.18e+03	2.38e-02	6.69e-02	2.55e-03	5.30e-02	3.23e-01	1.71e-02	9.07e-04	2.55e-06
Bolanos2009˙Fig9˙G6	1.23e+03	1.98e-01	6.41e-02	2.55e-03	4.42e-01	4.04e-02	1.79e-02	7.89e-03	1.54e-03
Bolanos2009˙Fig6˙O1	9.13e+02	4.60e-03	1.94e-02	2.50e-04	6.91e-02	1.24e-02	8.58e-04	5.93e-05	2.83e-07
Bolanos2009˙Fig6˙O3	9.37e+02	1.87e-02	2.02e-02	2.50e-04	2.72e-01	3.13e-03	8.51e-04	2.31e-04	1.71e-05
Bolanos2009˙Fig9˙G8	1.25e+03	8.14e-01	6.31e-02	2.55e-03	1.81e+00	1.00e-02	1.82e-02	3.29e-02	1.08e-01
Goldstein2010˙Fig5	1.22e+00	3.00e-03	2.00e-02	1.50e-02	1.57e-01	9.15e-02	1.43e-02	2.25e-03	5.53e-05

TABLE IV: Summary of the properties of all pinching experiments reproduced in the article: density ρ, viscosity η, surface tension Γ, extrinsic size D, Ohnesorge number $\mathrm{Oh} = \eta/(\rho\Gamma D)^{\frac{1}{2}}$, together with the values of the four time scales τ_{vi}, τ_{ic}, τ_{vc} and τ_o. The content of this table is available in the supplementary file '**DataSummary.csv**'.

II. VISCO-INERTIO-CAPILLARY SYSTEMS OF UNITS

In this section, we provide additional details on each of the four systems of units introduced in the article: visco-inertial (vi), visco-capillary (vc), inertio-capillary (ic) and Ohnesorge units (Oh).

A. Physical quantities

In the article we provided the characteristic length, time and mass scales associated with each system of units. From these quantities, the values of any quantity that can be expressed in units of mass, length and time can be derived. For instance, in the article we systematically gave the values of the stress $\Sigma = m.\ell^{-1}.\tau^{-2}$. In Table V we give the expressions for a few other quantities of interest.

Quantity	**vi units**	**vc units**	**ic units**	**Oh units**
Time τ	$\frac{\rho D^2}{\eta}$	$\frac{\eta D}{\Gamma}$	$\left(\frac{\rho D^3}{\Gamma}\right)^{\frac{1}{2}}$	$\frac{\eta^3}{\Gamma^2\rho}$
Length ℓ	D	D	D	$\frac{\eta^2}{\Gamma\rho}$
Mass m	ρD^3	$\frac{\eta^2 D^2}{\Gamma}$	ρD^3	$\frac{\eta^6}{\Gamma^3\rho^2}$
Viscosity	η	η	$(\rho\Gamma D)^{\frac{1}{2}}$	η
Surface tension	$\frac{\eta^2}{\rho D}$	Γ	Γ	Γ
Density	ρ	$\frac{\eta^2}{\Gamma D}$	ρ	ρ
Speed	$\frac{\eta}{\rho D}$	$\frac{\Gamma}{\eta}$	$\left(\frac{\Gamma}{\rho D}\right)^{\frac{1}{2}}$	$\frac{\Gamma}{\eta}$
Acceleration	$\frac{\eta^2}{\rho^2 D^3}$	$\frac{\Gamma^2}{\eta^2 D}$	$\frac{\Gamma}{\rho D^2}$	$\frac{\Gamma^3\rho}{\eta^4}$
Energy	$\frac{\eta^2 D}{\rho}$	ΓD^2	ΓD^2	$\frac{\eta^4}{\rho^2\Gamma}$
Force	$\frac{\eta^2}{\rho}$	ΓD	ΓD	$\frac{\eta^2}{\rho}$
Stress	$\frac{\eta^2}{\rho D^2}$	$\frac{\Gamma}{D}$	$\frac{\Gamma}{D}$	$\frac{\Gamma^2\rho}{\eta^2}$
Power	$\frac{\eta^3}{\rho^2 D}$	$\frac{\Gamma^2 D}{\eta}$	$\left(\frac{\Gamma^3 D}{\rho}\right)^{\frac{1}{2}}$	$\frac{\eta\Gamma}{\rho}$

TABLE V: Summary of the main physical quantities in the four systems of units used in the article.

B. Scaling regimes

In the article we mostly considered three simple scaling regimes (vi, vc and ic), and two non-trivial regimes, namely the size-dependent visco-capillary regime of Tanner's law and the size-dependent inertio-capillary regime of Rayleigh's law. These five regimes can be written in any of the four system of units as $d/\ell^* = Oh^\beta (t/\tau^*)^\alpha$, with $\tau^* = \gamma_1\tau$ and $\ell^* = \gamma_2\ell$, where τ and ℓ can be chosen from one of the four systems. Table VI give the values of Oh^β for each regime and choice of units. Note that the prefactors γ_1 and γ_2 take into account the dimensionless coefficients of the scaling laws (δ_{vc}, δ_{ic} etc) and will be discussed in section II E.

Schematic versions of the scaling regimes in vi, vc, ic and Oh units are given in SI-Fig. 1 to illustrate how the coordinates of the intersection points can be expressed from the Ohnesorge number.

Law	vi units	vc units	ic units	Oh units
$d \propto \left(\frac{\eta}{\rho}\right)^{\frac{1}{2}} t^{\frac{1}{2}}$	1	Oh	$\mathrm{Oh}^{\frac{1}{2}}$	1
$d \propto \frac{\Gamma}{\eta} t$	Oh^{-2}	1	Oh^{-1}	1
$d = \left(\frac{\Gamma}{\rho}\right)^{\frac{1}{3}} t^{\frac{2}{3}}$	$\mathrm{Oh}^{-\frac{2}{3}}$	$\mathrm{Oh}^{\frac{2}{3}}$	1	1
$d \propto \left(\frac{\Gamma D^9}{\eta}\right)^{\frac{1}{10}} t^{\frac{1}{10}}$	$\mathrm{Oh}^{-\frac{1}{5}}$	1	$\mathrm{Oh}^{-\frac{1}{10}}$	$\mathrm{Oh}^{-\frac{9}{5}}$
$d \propto \left(\frac{\Gamma D}{\rho}\right)^{\frac{1}{4}} t^{\frac{1}{2}}$	$\mathrm{Oh}^{-\frac{1}{2}}$	$\mathrm{Oh}^{\frac{1}{2}}$	1	$\mathrm{Oh}^{-\frac{1}{2}}$

TABLE VI: Ohnesorge-based prefactors for the five main scaling laws discussed in the article. For instance, $d \propto (\Gamma/\eta)t$ can be written as $d/\ell_{vi} \propto \mathrm{Oh}^{-2}(t/\tau_{vi})$, or $d/\ell_{vc} \propto t/\tau_{vc}$, or $d/\ell_{ic} \propto \mathrm{Oh}^{-1}(t/\tau_{ic})$, or $d/\ell_o \propto t/\tau_o$.

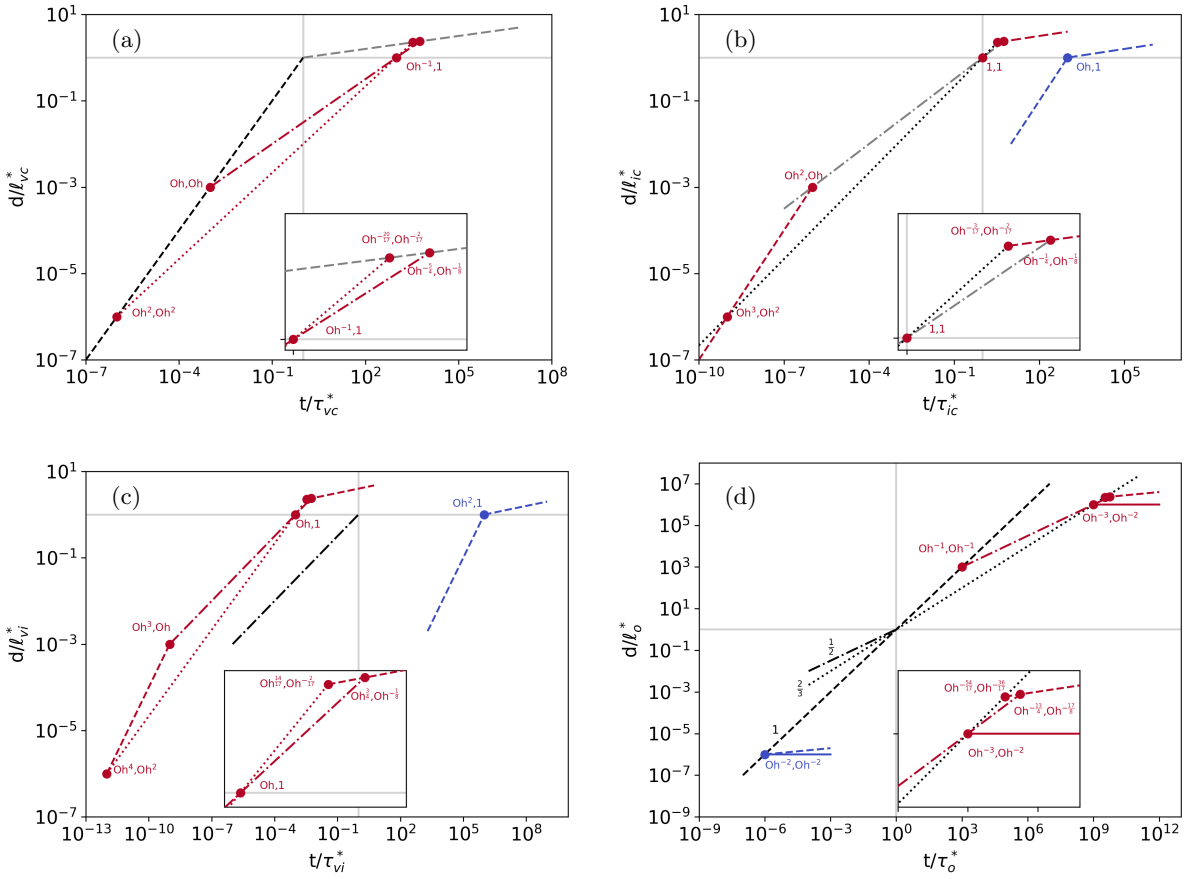

FIG. 1: Schematic plots of the main scaling laws discussed in the article, together with the coordinates of the their intersections, expressed in terms of the Ohnesorge number Oh. In each panel, the inset provides a close-up on the intersection between the $\frac{2}{3}$ regime, Rayleigh's $\frac{1}{2}$ regime and Tanner's $\frac{1}{10}$ regime. Note that the precision provided by current experiments does not offer ways to confirm or inform the slight differences between the intersections of the $\frac{1}{2}$ or $\frac{2}{3}$ regime with Tanner's law. For instance, for the visco-capillary units the intersection of the $\frac{2}{3}$ and $\frac{1}{10}$ regime is given by $t/\tau^*_{vc} = \mathrm{Oh}^{-\frac{20}{17}} = \mathrm{Oh}^{-\frac{5}{4}}\mathrm{Oh}^{\frac{5}{68}}$ and $d/\ell^*_{vc} = \mathrm{Oh}^{-\frac{2}{17}} = \mathrm{Oh}^{-\frac{1}{8}}\mathrm{Oh}^{\frac{1}{136}}$, which are here expressed from the coordinates of the intersection between the $\frac{1}{2}$ and $\frac{1}{10}$ regimes. Since these intersections are meaningful if $\mathrm{Oh} < 1$, the corrections factors $\mathrm{Oh}^{\frac{5}{68}}$ and $\mathrm{Oh}^{\frac{1}{136}}$ are always close to 1. The color of each curve gives the value of Oh (see Fig. 5 of main article).

C. Supplementary figures in vi, vc and ic units

In this section we give different versions of the visco-capillary, inertio-capillary and visco-inertial plots of the article highlighting subsets of the data.

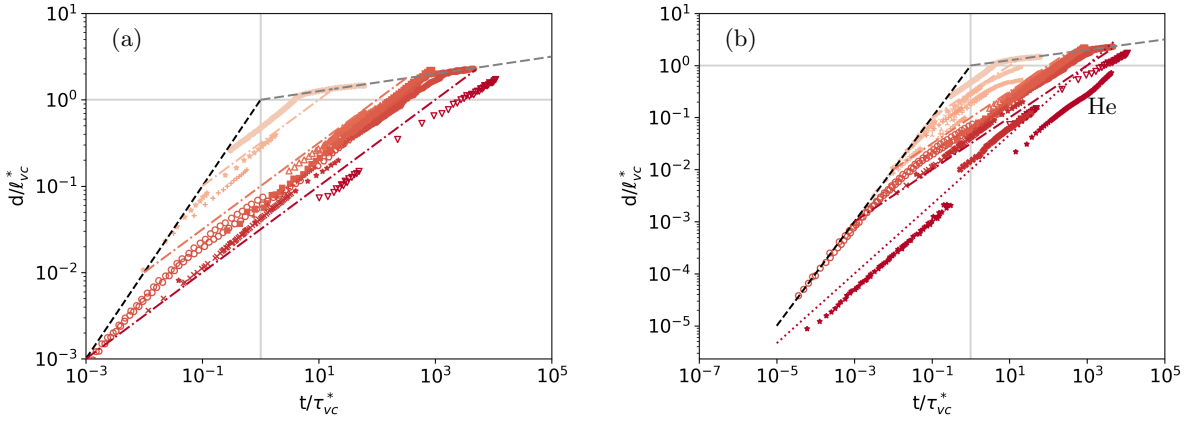

FIG. 2: Supplementary visco-capillary plots. (a) Data from Fig. 2c of the article, replotted in visco-capillary units. The three dashed lines follow Rayleigh's regime $d/\ell^*_{vc} = \mathrm{Oh}^{\frac{1}{2}}(t/\tau^*_{vc})^{\frac{1}{2}}$, for $\mathrm{Oh} = 10^{-1}$, 10^{-2} and 10^{-3}. (b) Data from Fig. 2d of the article, replotted in visco-capillary units. In addition to the the three dashed lines following Rayleigh's regime, the dotted line follows the inertio-capillary regime $d/\ell^*_{vc} = \mathrm{Oh}^{\frac{2}{3}}(t/\tau^*_{vc})^{\frac{1}{2}}$, for $\mathrm{Oh} = 10^{-3}$. The data set labeled 'He' corresponds to superfluid Helium, for which a viscosity is unavailable. We artificially set $\eta = 10^{-6}$ Pa.s in order to represent the data on the visco-capillary plot. If $\eta \simeq 0$, the actual abscissa on this set should be infinite. It is probably more reasonable to assume that an effective viscosity would set in, due to a different dissipation mechanism [2]. The color of each curve gives the value of Oh (see Fig. 5 of the main article).

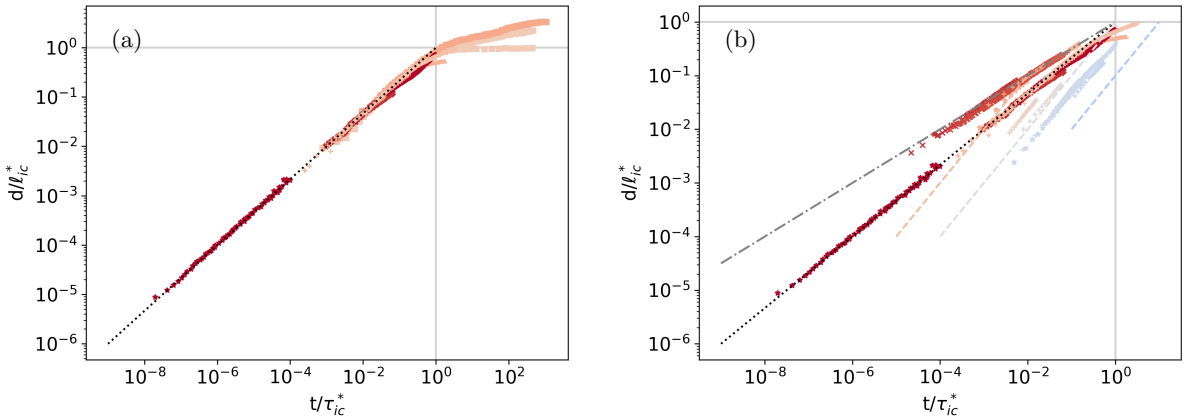

FIG. 3: Supplementary inertio-capillary plots. (a) All spreading, coalescence and pinching experiments reproduced in the article exhibiting a $\frac{2}{3}$ regime are replotted in inertio-capillary units (see Tables VII-IX for values of δ_{ic}). (b) All pinching experiments replotted in visco-capillary units. In addition to Rayleigh's regime (dotted-dashed line) and to the inertio-capillary regime (dotted line), the dashed lines follow the visco-capillary regime $d/\ell^*_{ic} = \mathrm{Oh}^{-1}(t/\tau^*_{ic})$, for $\mathrm{Oh} = 10^{-1}$, 1, 10^1. The color of each curve gives the value of Oh (see Fig. 5 of the main article).

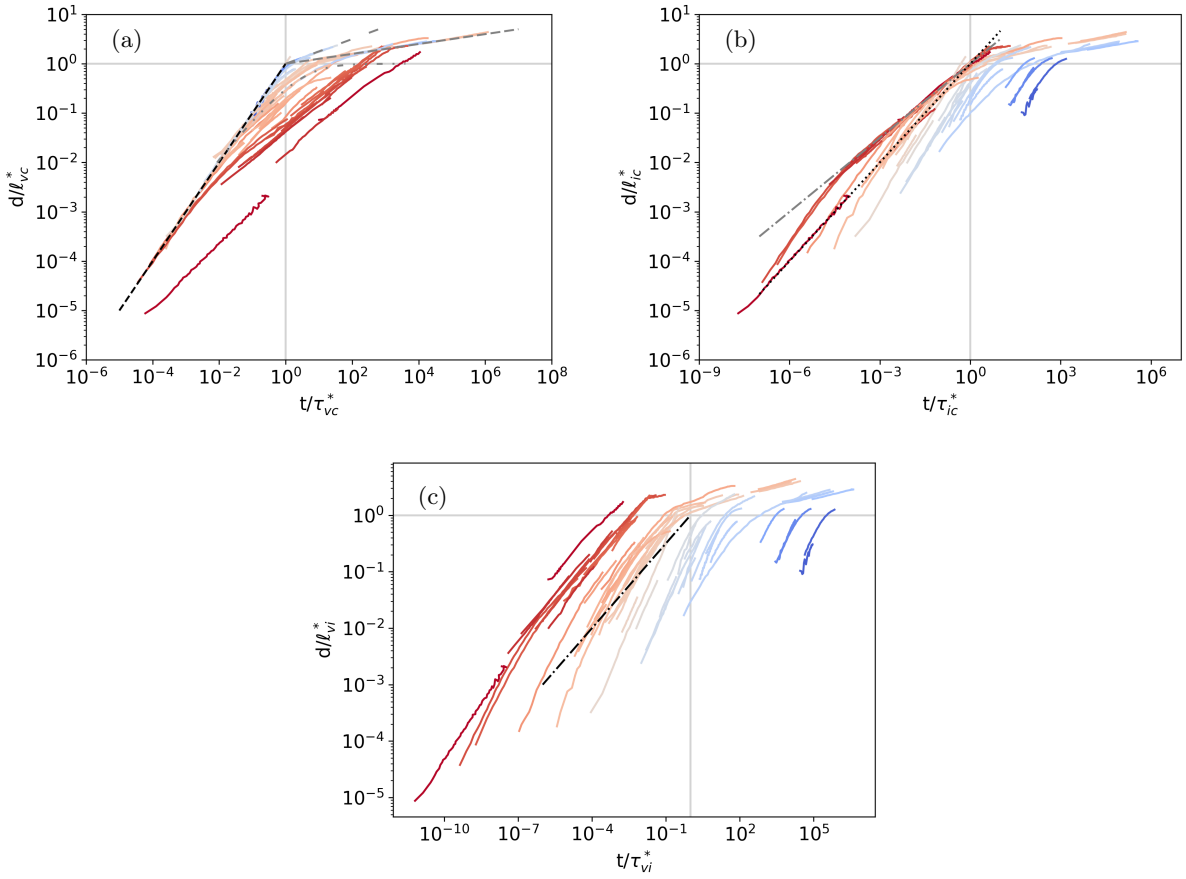

FIG. 4: All data sets from Fig. 5 of the main article reproduced in visco-capillary, inertio-capillary and visco-inertial units. See extended legend and animated figures for details. The color of each curve gives the value of Oh (see Fig. 5 of the main article).

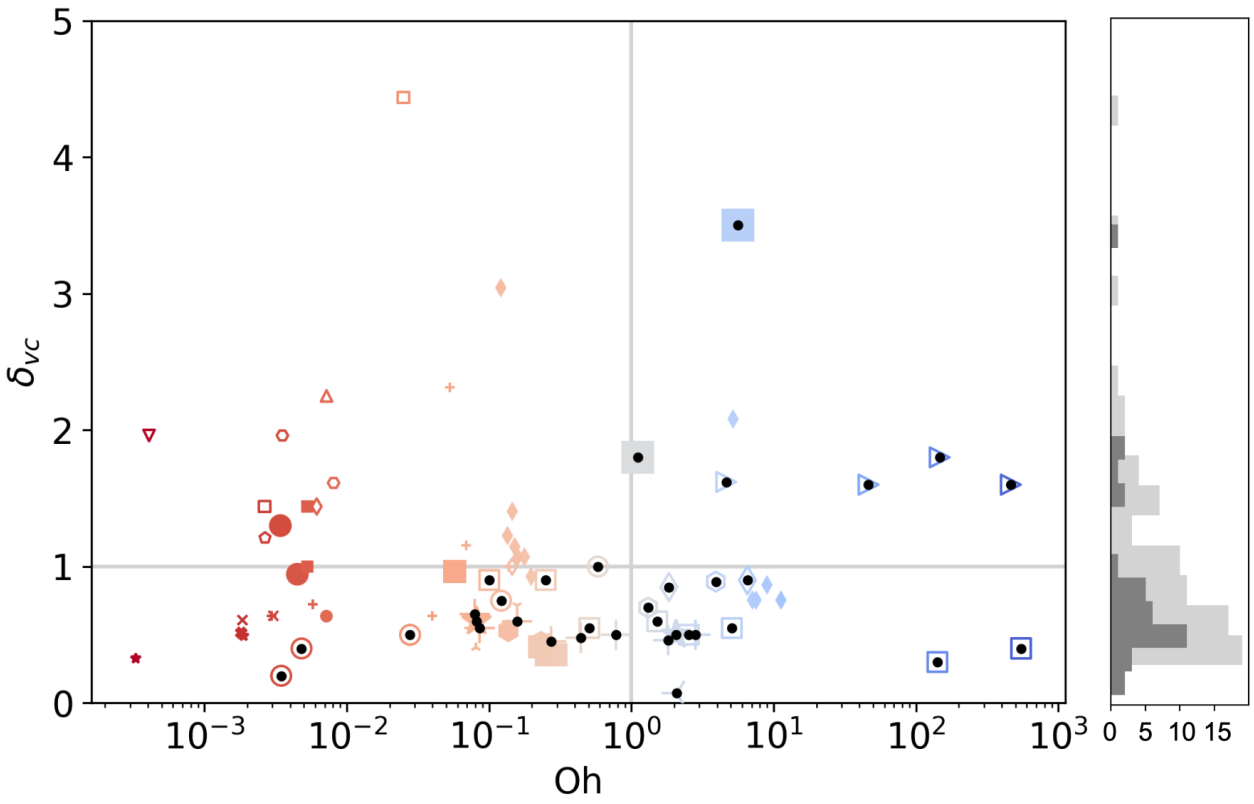

FIG. 5: Measurements of the values of the purely visco-capillary prefactors δ_{vc} as a function of the Ohnesorge number, for all experiments reproduced in the article. (Left) The biggest symbols with the added black dots correspond to direct measurements of δ_{vc} from fitting a linear regime present on the data. The medium-size symbols correspond to indirect measurements of δ_{vc} from two other prefactors (see section II F). The smallest symbols correspond to indirect measurements from a single other prefactor (least reliable). (Right) Distribution of the values of δ_{vc}, for direct measurements (dark gray) and all measurements (light gray).

D. Dimensionless constants

All scaling regimes introduced in the article include dimensionless prefactors. For instance, the simple visco-capillary regime is $d = \delta_{vc}\Gamma t/\eta$. The prefactor δ_{vc} is expected to be a 'constant of order 1', which more rigorously means that the variations of δ_{vc} with d, t, η or Γ can be at most logarithmic. This assumption that can be verified experimentally. For all experiments presenting a linear scaling $d \sim t$, we computed the value of δ_{vc} that better fitted the data. The values of δ_{vc} in all cases where the linear regime was present are given for spreading, coalescence and pinching in Tables VII, VIII and IX. The value of δ_{vc} appears to be independent of the Ohnesorge number, as shown in SI-Fig. 5. Only considering direct measurements the most frequent value (mode) is $\delta_{vc} \simeq 0.5$ and the mean is $\delta_{vc} \simeq 0.9$ (see Fig. 5 for full distribution). We will show in section II F how additional values of δ_{vc} can be inferred from the prefactors of other scaling laws.

The values of δ_{ic}, δ_{Tan} and δ_{Ray} obtained from experiments are shown in SI-Fig. 6. All values are indeed of order 1 and seem quite independent of the Ohnesorge number. When possible, the values of the measured prefactors are given in Tables VII, VIII and IX.

E. Unit prefactors

In all figures of the article, the units of length and time take into account the dimensionless constants (δ_{vc}, δ_{ic} etc) included in the various scaling laws. For instance, in Fig. 5 giving the dynamics in Ohnesorge units, the axes are t/τ_o^* and d/ℓ_o^*, where $\tau_o^* \equiv \gamma_1\tau_o$ and $\ell_o^* \equiv \gamma_2\ell_o$. In all figures associated with the four systems of units, the values of γ_1 and γ_2 for a particular data set are identical. The values of γ_1, γ_2 are given for spreading, coalescence and pinching data in Tables VII, VIII and IX and in Fig. 7. In this section we discuss how the values of γ_1 and γ_2 are computed.

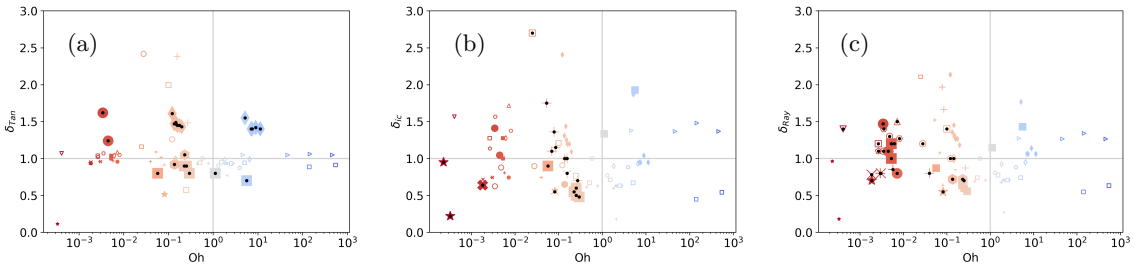

FIG. 6: Values of dimensionless constants δ_{Tan}, δ_{ic} and δ_{Ray}, from direct fits of experimental data presenting the appropriate scalings (big symbols with black dots), and from indirect measurements (smaller symbols; see section II F).

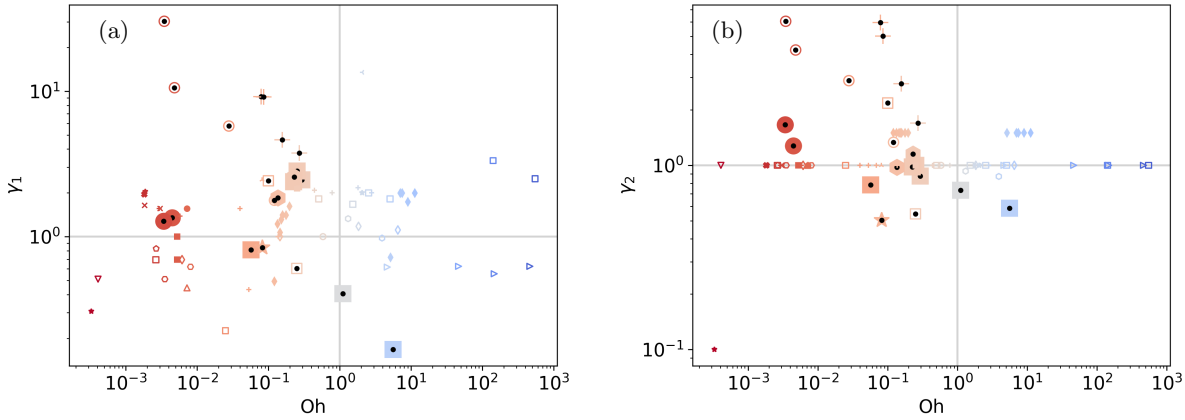

FIG. 7: Values of the dimensionless prefactors γ_1 and γ_2 used for any of the four systems of units. The big data points with black dots correspond to direct measurements from fitting two consecutive regimes. The smaller data points correspond to values inferred from fitting a single regime.

Let us take as an example a case of dynamics abiding to the simple visco-capillary scaling:

$$d = \delta_{vc}\frac{\Gamma}{\eta}t \leftrightarrow \frac{d}{\ell_{vi}} = \delta_{vc}\mathrm{Oh}^{-2}\frac{t}{\tau_{vi}} \leftrightarrow \frac{d}{\ell_{vc}} = \delta_{vc}\frac{t}{\tau_{vc}} \leftrightarrow \frac{d}{\ell_{ic}} = \delta_{vc}\mathrm{Oh}^{-1}\frac{t}{\tau_{ic}} \leftrightarrow \frac{d}{\ell_{o}} = \delta_{vc}\frac{t}{\tau_{o}} \tag{1}$$

The goal of the coefficients γ_1 and γ_2 is to factor in the value of δ_{vc}, such that the regime can be written as

$$\frac{d}{\ell^*_{vi}} = \mathrm{Oh}^{-2}\frac{t}{\tau^*_{vi}} \leftrightarrow \frac{d}{\ell_{vc^*}} = \frac{t}{\tau^*_{vc}} \leftrightarrow \frac{d}{\ell^*_{ic}} = \mathrm{Oh}^{-1}\frac{t}{\tau^*_{ic}} \leftrightarrow \frac{d}{\ell^*_{o}} = \frac{t}{\tau^*_{o}} \tag{2}$$

Regardless of the system of units, the constraint on γ_1 and γ_2 is the same:

$$\frac{\delta_{vc}\gamma_1}{\gamma_2} = 1 \tag{3}$$

Let us now assume that the data set first follows the simple visco-capillary regime and then displays Rayleigh's regime. In that case, the second regime provides an additional constraint:

$$\frac{\delta_{Ray}\gamma_1^{\frac{1}{2}}}{\gamma_2} = 1 \tag{4}$$

Solving the system made of Eq. 3 and Eq. 4 would lead to:

$$\gamma_1 = \left(\frac{\delta_{Ray}}{\delta_{vc}}\right)^2 \tag{5}$$

$$\gamma_2 = \frac{\delta^2_{Ray}}{\delta_{vc}} \tag{6}$$

For all experimental data sets presenting two consecutive regimes, we followed the procedure outlined in the example above in order to obtain the values of γ_1 and γ_2. We encountered five cases summarized here:

$$\text{- input: } \delta_{vc} \text{ and } \delta_{Tan} \rightarrow \gamma_1 = \left(\frac{\delta_{Tan}}{\delta_{vc}}\right)^{\frac{10}{9}} \text{ and } \gamma_2 = \delta_{vc}\gamma_1 \tag{7}$$

$$\text{- input: } \delta_{vc} \text{ and } \delta_{ic} \rightarrow \gamma_1 = \left(\frac{\delta_{ic}}{\delta_{vc}}\right)^{3} \text{ and } \gamma_2 = \delta_{vc}\gamma_1 \tag{8}$$

$$\text{- input: } \delta_{vc} \text{ and } \delta_{Ray} \rightarrow \gamma_1 = \left(\frac{\delta_{Ray}}{\delta_{vc}}\right)^{2} \text{ and } \gamma_2 = \delta_{vc}\gamma_1 \tag{9}$$

$$\text{- input: } \delta_{Tan} \text{ and } \delta_{ic} \rightarrow \gamma_1 = \left(\frac{\delta_{Tan}}{\delta_{ic}}\right)^{\frac{30}{17}} \text{ and } \gamma_2 = \delta_{ic}\gamma_1^{\frac{2}{3}} \tag{10}$$

$$\text{- input: } \delta_{Tan} \text{ and } \delta_{Ray} \rightarrow \gamma_1 = \left(\frac{\delta_{Tan}}{\delta_{Ray}}\right)^{\frac{5}{2}} \text{ and } \gamma_2 = \delta_{Ray}\gamma_1^{\frac{1}{2}} \tag{11}$$

$$\tag{12}$$

In some experiments only a single regime is available, in which case we chose to set $\gamma_2 = 1$ and use the prefactor of the regime to obtain a value of γ_1. For instance, for the spreading experiment labeled 'Eddi2013 Fig6 water', the data only show Rayleigh's regime, giving $\delta_{Ray} = 1.2$, and we set $\gamma_2 = 1$ to get $\gamma_1 = 1/\delta_{Ray}^2 \simeq 0.69$. In all these cases presenting a single regime, the values of γ_1 and γ_2 must be understood as quite approximate. In two cases we chose slightly different values of γ_2. In coalescence experiments by Yokota *et al.* the confinement between two plates leads to a late spreading abiding to $d/\tau_{vc} \propto (t/\tau_{vc})^{\frac{1}{4}}$, and the values of γ_2 are chosen to comply with this regime. The second example where we chose $\gamma_2 \neq 1$ concerns the Tanner regime studied by Cazabat *et al.*. In that case, the sole constraint is:

$$\gamma_1 = \left(\frac{\gamma_2}{\delta_{Tan}}\right)^{10} \rightarrow \frac{\Delta\gamma_1}{\gamma_1} = 10\frac{\Delta\gamma_2}{\gamma_2} + 10\frac{\Delta\delta_{Tan}}{\delta_{Tan}} \tag{13}$$

In the right-hand side we express the relative uncertainty on γ_1 based on the uncertainty on γ_2 and δ_{Tan}. Even if we assume that the uncertainty on δ_{Tan} obtained from fitting data is negligible, small variations of γ_2 can lead to substantial variations of γ_1. For Cazabat's data, choosing $\gamma_2 = 1$ led to unreasonable values of γ_1 so we took the liberty of slightly tuning γ_2 in order to recover values in accordance with the other data sets. This was done by deriving the inferred value of δ_{vc}, as we shall explain now.

Label	**Oh**	$\boldsymbol{\delta_{vc}}$	$\boldsymbol{\delta_{Tan}}$	$\boldsymbol{\delta_{ic}}$	$\boldsymbol{\delta_{Ray}}$	$\boldsymbol{\gamma_1}$	$\boldsymbol{\gamma_2}$
Cazabat1986˙Fig1a˙0p78	1.97e-01	nan	1.43	nan	nan	1.61	1.50
Cazabat1986˙Fig1a˙1p5	1.77e-01	nan	1.45	nan	nan	1.40	1.50
Cazabat1986˙Fig1a˙2p9	1.59e-01	nan	1.45	nan	nan	1.40	1.50
Cazabat1986˙Fig1a˙3p8	1.52e-01	nan	1.46	nan	nan	1.31	1.50
Cazabat1986˙Fig1a˙4p7	1.46e-01	nan	1.49	nan	nan	1.07	1.50
Cazabat1986˙Fig1a˙7p8	1.34e-01	nan	1.47	nan	nan	1.22	1.50
Cazabat1986˙Fig1a˙14p4	1.21e-01	nan	1.61	nan	nan	0.49	1.50
Cazabat1986˙Fig1b˙37p9	5.16e+00	nan	1.55	nan	nan	0.72	1.50
Cazabat1986˙Fig1b˙5p8	7.06e+00	nan	1.4	nan	nan	1.99	1.50
Cazabat1986˙Fig1b˙4p03	7.50e+00	nan	1.4	nan	nan	1.99	1.50
Cazabat1986˙Fig1b˙1p35	9.00e+00	nan	1.42	nan	nan	1.73	1.50
Cazabat1986˙Fig1b˙0p35	1.13e+01	nan	1.4	nan	nan	1.99	1.50
Biance2004˙Fig3˙0p27	7.17e-03	nan	nan	nan	0.8	1.56	1.00
Biance2004˙Fig3˙0p7	4.45e-03	nan	1.24	nan	1.1	1.35	1.28
Biance2004˙Fig3˙1p2	3.40e-03	nan	1.62	nan	1.47	1.27	1.66
Eddi2013˙Fig4˙0p37	2.95e-01	nan	0.8	0.48	nan	2.46	0.88
Eddi2013˙Fig4˙0p5	2.53e-01	nan	0.9	0.5	nan	2.82	1.00
Eddi2013˙Fig4˙0p63	2.26e-01	nan	0.9	0.55	nan	2.38	0.98
Eddi2013˙Fig5a˙105deg	2.53e-01	nan	nan	0.6	nan	2.15	1.00
Eddi2013˙Fig5b˙0	5.28e-03	nan	nan	nan	1.2	0.69	1.00
Eddi2013˙Fig5b˙115	5.28e-03	nan	nan	nan	1	1.00	1.00
Eddi2013˙Fig6˙water	5.28e-03	nan	nan	nan	1.2	0.69	1.00
Eddi2013˙Fig6˙11	5.71e-02	nan	0.8	0.9	nan	0.81	0.78
Eddi2013˙Fig6˙1120	5.61e+00	3.5	0.7	nan	nan	0.17	0.59
Eddi2013˙Fig6˙220	1.11e+00	1.8	0.8	nan	nan	0.41	0.73
Chen2014˙Fig3b˙60cP	2.31e-01	nan	1.05	nan	0.72	2.57	1.15
Chen2014˙Fig3b˙35p5cP	1.36e-01	nan	0.92	nan	0.72	1.85	0.98

TABLE VII: Summary of the values of the dimensionless prefactors for all spreading experiments reproduced in the article. The content of this table is available in the supplementary file '**DataSummary.csv**'.

Label	**Oh**	δ_{vc}	δ_{Tan}	δ_{ic}	δ_{Ray}	γ_1	γ_2
Menchaca2001˙Fig9	4.08e-04	nan	nan	nan	1.4	0.51	1.00
Wu2004˙Fig4˙1p94	2.67e-03	nan	nan	nan	1.1	0.83	1.00
Yao2005˙100000cS˙5cm	1.47e+02	1.8	nan	nan	nan	0.56	1.00
Yao2005˙100000cS˙0p5cm	4.64e+02	1.6	nan	nan	nan	0.62	1.00
Yao2005˙10000cS˙0p5cm	4.64e+01	1.6	nan	nan	nan	0.62	1.00
Yao2005˙1000cS˙0p5cm	4.64e+00	1.62	nan	nan	nan	0.62	1.00
Thoroddsen2005˙Fig6	3.53e-03	nan	nan	nan	1.4	0.51	1.00
Thoroddsen2005b˙Fig4	8.08e-03	nan	nan	nan	1.27	0.62	1.00
Aarts2005˙Fig2˙100mPas	5.08e-01	0.55	nan	nan	nan	1.82	1.00
Aarts2005˙Fig2˙1Pas	5.08e+00	0.55	nan	nan	nan	1.82	1.00
Aarts2005˙Fig2˙500mPas	2.54e+00	0.5	nan	nan	nan	2.00	1.00
Aarts2005˙Fig2˙300mPas	1.52e+00	0.6	nan	nan	nan	1.67	1.00
Aarts2005˙Fig3˙5mPas	2.50e-02	nan	nan	2.7	nan	0.23	1.00
Aarts2005˙Fig3˙20mPas	1.00e-01	0.9	nan	nan	1.4	2.42	2.18
Aarts2005˙Fig3˙50mPas	2.50e-01	0.9	nan	nan	0.7	0.60	0.54
Aarts2005˙Fig3˙1mPas	2.64e-03	nan	nan	nan	1.2	0.69	1.00
Aarts2008˙Fig9˙bubb17	1.42e+02	0.3	nan	nan	nan	3.33	1.00
Aarts2008˙Fig9˙drop17	5.50e+02	0.4	nan	nan	nan	2.50	1.00
Yokota2011˙Fig2˙289	1.31e+00	0.7	nan	nan	nan	1.33	0.93
Yokota2011˙Fig2˙888	3.92e+00	0.89	nan	nan	nan	0.98	0.87
Paulsen2011˙Fig2˙1p9	4.81e-03	0.4	nan	nan	1.3	10.56	4.23
Paulsen2011˙Fig2˙11	2.79e-02	0.5	nan	nan	1.2	5.76	2.88
Paulsen2011˙Fig2˙48	1.22e-01	0.75	nan	nan	1.0	1.78	1.33
Paulsen2011˙Fig2˙230	5.82e-01	1	nan	nan	nan	1.00	1.00
Paulsen2014˙Fig1	3.46e-03	0.2	nan	nan	1.1	30.25	6.05
Soto2018˙Fig5	7.21e-03	nan	nan	nan	1.5	0.44	1.00
Rahman2019˙Fig6˙6p65	6.54e+00	0.9	nan	nan	nan	1.11	1.00
Rahman2019˙Fig6˙1p84	1.84e+00	0.85	nan	nan	nan	1.18	1.00
Rahman2019˙Fig6˙0p146	1.45e-01	nan	nan	nan	1	1.00	1.00
Rahman2019˙Fig6˙0p00692	6.15e-03	nan	nan	nan	1.2	0.69	1.00

TABLE VIII: Summary of the values of the dimensionless prefactors for all coalescence experiments reproduced in the article. The content of this table is available in the supplementary file '**DataSummary.csv**'.

Label	**Oh**	$\boldsymbol{\delta_{vc}}$	$\boldsymbol{\delta_{Tan}}$	$\boldsymbol{\delta_{ic}}$	$\boldsymbol{\delta_{Ray}}$	$\boldsymbol{\gamma_1}$	$\boldsymbol{\gamma_2}$
Chen1997˙Fig7	8.11e-02	nan	nan	0.55	nan	2.45	1.00
McKinley2000˙Fig4	2.08e+00	0.074	nan	nan	nan	13.51	1.00
Chen2002˙Fig3	1.81e-03	nan	nan	0.64	nan	1.95	1.00
Burton2004˙Fig5	3.30e-04	nan	nan	0.22	nan	0.31	0.10
Burton2005˙0p9	1.88e-03	nan	nan	nan	0.7	2.04	1.00
Burton2005˙37p4	8.20e-02	0.6	nan	nan	0.55	0.84	0.50
Burton2005˙1011	2.06e+00	0.5	nan	nan	nan	2.00	1.00
Burton2007˙Fig7	nan	nan	nan	0.95	nan	1.08	1.00
Keim2006˙Fig2˙4p1	1.84e-03	nan	nan	nan	0.78	1.64	1.00
Keim2006˙Fig2˙1p5	3.04e-03	nan	nan	nan	0.8	1.56	1.00
Bolanos2009˙Fig6˙water	5.76e-03	nan	nan	nan	0.85	1.38	1.00
Bolanos2009˙Fig7˙water	2.95e-03	nan	nan	nan	0.8	1.56	1.00
Bolanos2009˙Fig6˙O2	1.37e-01	nan	nan	1	nan	1.00	1.00
Bolanos2009˙Fig7˙O7	3.99e-02	nan	nan	nan	0.8	1.56	1.00
Bolanos2009˙Fig7˙O8	7.89e-02	0.65	nan	1.36	nan	9.16	5.95
Bolanos2009˙Fig7˙O9	1.57e-01	0.6	nan	1.0	nan	4.63	2.78
Bolanos2009˙Fig8˙G1	8.57e-02	0.55	nan	1.15	nan	9.14	5.03
Bolanos2009˙Fig8˙G2	7.80e-01	0.5	nan	nan	nan	2.00	1.00
Bolanos2009˙Fig8˙G4	2.81e+00	0.5	nan	nan	nan	2.00	1.00
Bolanos2009˙Fig9˙G5	5.30e-02	nan	nan	1.75	nan	0.43	1.00
Bolanos2009˙Fig9˙G6	4.42e-01	0.48	nan	nan	nan	2.08	1.00
Bolanos2009˙Fig6˙O1	6.91e-02	nan	nan	1.1	nan	0.87	1.00
Bolanos2009˙Fig6˙O3	2.72e-01	0.45	nan	0.7	nan	3.76	1.69
Bolanos2009˙Fig9˙G8	1.81e+00	0.46	nan	nan	nan	2.17	1.00
Goldstein2010˙Fig5	1.57e-01	nan	nan	0.8	nan	1.40	1.00

TABLE IX: Summary of the values of the dimensionless prefactors for all pinching experiments reproduced in the article. The content of this table is available in the supplementary file '**DataSummary.csv**'.

F. Consistency relations

In all data we collected on spreading, coalescence and pinching, we never encountered a set presenting three consecutive regimes. However, such dynamics are absolutely possible. For instance, a spreading with a low value of Ohnesorge number could first follow the linear visco-capillary regime, then follow Rayleigh's regime and finally reach Tanner's regime. The data from Biance *et al.* encompass the last two regimes ($\frac{1}{2}$ and $\frac{1}{10}$) but lack enough time resolution to describe the initial visco-capillary regime. If future experiments manage to resolve three consecutive regimes, one could check consistency relationships between the different prefactors. For instance, in the case outlined above, the three consecutive regimes would lead to the following constraints on γ_1 and γ_2:

$$\begin{cases} \gamma_2 &= \delta_{vc}\gamma_1 \\ \gamma_2 &= \delta_{Ray}\gamma_1^{\frac{1}{2}} \\ \gamma_2 &= \delta_{Tan}\gamma_1^{\frac{1}{10}} \end{cases} \rightarrow \delta_{Ray}^9 = \delta_{vc}^4\delta_{Tan}^5 \tag{14}$$

The constraints impose that the three constant prefactors are not independent and must respect the equation on the right-hand side. We have used such consistency equations to infer values of prefactors inaccessible in experiments. For instance, from Biance's data providing values for δ_{Ray} and δ_{Tan}, we computed the predicted values of $\delta_{vc} = (\delta_{Ray}^9/\delta_{Tan}^5)^{\frac{1}{4}}$. These inferred values are present as the two red dots in SI-Fig. 5, corresponding to 'Biance2004 Fig3 0p7' and 'Biance2004 Fig3 1p2'.

In general, if values of γ_1 and γ_2 are provided, the values of the constant prefactors can be inferred using the following equations:

$$\delta_{vc} = \frac{\gamma_2}{\gamma_1} \tag{15}$$

$$\delta_{Tan} = \frac{\gamma_2}{\gamma_1^{\frac{1}{10}}} \tag{16}$$

$$\delta_{ic} = \frac{\gamma_2}{\gamma_1^{\frac{2}{3}}} \tag{17}$$

$$\delta_{Ray} = \frac{\gamma_2}{\gamma_1^{\frac{1}{2}}} \tag{18}$$

$$\tag{19}$$

These relations allow to infer values of the prefactors in all cases, even if a particular experiment is not expected to display a given regime. For instance, for a coalescence experiment, Tanner's regime is irrelevant, but a hypothetical value of δ_{Tan} can be computed anyway. All indirect measurements of prefactors in SI-Fig. 5 and 6 are obtained using the equations given above.

III. CATEGORIES OF DIMENSIONLESS NUMBERS

The article aims at analyzing dynamics based on four dimensional parameters: three materials parameters (ρ, η and Γ) and one geometric parameter D. We call these quantities 'parameters' because they are expected to be constant for a particular experiment, in contrast to the variables d and t. These four dimensional parameters and the associated two dimensional variables can combine to produce a variety of quantities without dimensions. According to dimensional analysis, the dynamics can be fully characterized by 3 dimensionless numbers (6 quantities -3 dimensions) [3]. In the article we favored descriptions based on four different choices of dimensionless times and lengths in conjunction with the Ohnesorge number. In this section, we entertain different approaches and try to categorize the different kinds of dimensionless numbers in the hope to facilitate comparison with different viewpoints.

In the article, we encounter a few kinds of quantities without dimensions, which we shall summarize here and comment thereafter.

- Scaling exponents: any scaling regime $d = Kt^\alpha$ is associated with a dimensionless exponent α.

- Simple dynamic dimensionless numbers: Re, Ca, We.

- Variable geometric ratio: Λ.

- Dimensionless constants: δ_{vi}, δ_{vc}, δ_{ic}, δ_{Tan}, δ_{Ray}.

- Ohnesorge and Laplace numbers: Oh, La.
- Dimensionless lengths: d/ℓ_{vi}, d/ℓ_{vc}, d/ℓ_{ic}, d/ℓ_o.
- Dimensionless times: t/τ_{vi}, d/τ_{vc}, d/τ_{ic}, d/τ_o.
- Dimensionless unit prefactors: γ_1, γ_2.

A. Scaling exponents

In the article we discussed five main scaling laws, associated with the exponents 1 (vc), $\frac{1}{2}$ (vi and Rayleigh), $\frac{2}{3}$ (ic) and $\frac{1}{10}$ (Tanner). The values of these exponents are connected to the dimensions of the components of the prefactor K in $d = Kt^\alpha$. For instance, $\alpha = \frac{2}{3}$ for the inertio-capillary regime because $[K] = ([\Gamma]/[\rho])^{\frac{1}{3}} = \mathcal{L}.\mathcal{T}^{-\frac{2}{3}}$. Since physical quantities tend to have dimensions $\mathcal{M}^a.\mathcal{L}^b.\mathcal{T}^c$, with a, b and c small integers, then scaling exponents with a mechanical underpinning can only be rational numbers built from ratios of small integers. However, if one adds logarithmic corrections as in $d \propto Kt^\alpha \log(d/D)$, then the apparent scaling exponent may deviate from simple fractions. In that case, one can define the apparent exponent as the logarithmic derivative [4]:

$$\alpha_* \equiv \frac{\partial \log d}{\partial \log t} \tag{20}$$

In theory one may derive the evolution of the apparent exponent $\alpha_*(t)$ for all dynamics reported in the article. In practice, the use of a derivative can introduce a substantial source of error. In SI-Fig. 8a we give the computed apparent exponent for an example of spreading from Eddi *et al.* [4], obtained with different methods of derivation.

B. Simple dynamic dimensionless numbers

Although without dimensions, the scaling exponents are usually not considered as dimensionless numbers per say. Traditional dimensionless numbers are understood as ratios of dimensional quantities. What we call a 'simple dimensionless number' is a ratio built from two material parameters with dimensions of the form $\mathcal{M}.\mathcal{L}^b.\mathcal{T}^c$, and a kinematic quantity with dimensions $\mathcal{L}^{b'}.\mathcal{T}^{c'}$. Following standard definitions, the article introduced three such simple dimensionless numbers:

$$\mathrm{Re} \equiv \frac{\rho d v}{\eta} = \frac{dv}{\nu} \tag{21}$$

$$\mathrm{Ca} \equiv \frac{\eta v}{\Gamma} = \frac{v}{c} \tag{22}$$

$$\mathrm{We} \equiv \frac{\rho d v^2}{\Gamma} = \frac{dv^2}{\kappa} \tag{23}$$

These definitions are rooted in steady hydrodynamics, where d and v are usually understood as control parameters imposed by the experimenter. Here d and v are the variable extent and speed of the spreading/coalescing/pinching object. Hence, the dimensionless numbers Re, Ca and We are dynamical, in the sense that their values can change over the course of an experiment. Computation of the values of the simple dimensionless numbers is contingent on deriving the leading edge speed:

$$v \equiv \frac{\partial d}{\partial t} = \alpha_* \frac{d}{t} \tag{24}$$

In SI-Fig. 8b we give the edge speed computed from simple differences without any additional processing, the ratio d/t and the curve $d(t)$ for the example 'Eddi2013 Fig6 220' [4]. From this perspective, the apparent scaling exponent can be defined as a ratio of two speeds: $\alpha_* = vt/d$. The result of this definition is given as the yellow curve in SI-Fig. 8a.

For a given data set $d(t)$, the values of Re, Ca and We can be computed at any time after deriving the speed v, as shown on an example in SI-Fig. 8. If the Reynolds number is constant it means that $d \sim t^{\frac{1}{2}}$. If the Capillary number is constant it means that $d \sim t$. If the Weber number is constant it means that $d \sim t^{\frac{2}{3}}$. In this example, the dynamics first seem to display a constant Weber number, and indeed $\alpha_* \simeq \frac{2}{3}$, as show in SI-Fig. 8a. The value of the constant will be connected to the dimensionless numbers δ_{ic} in section III D.

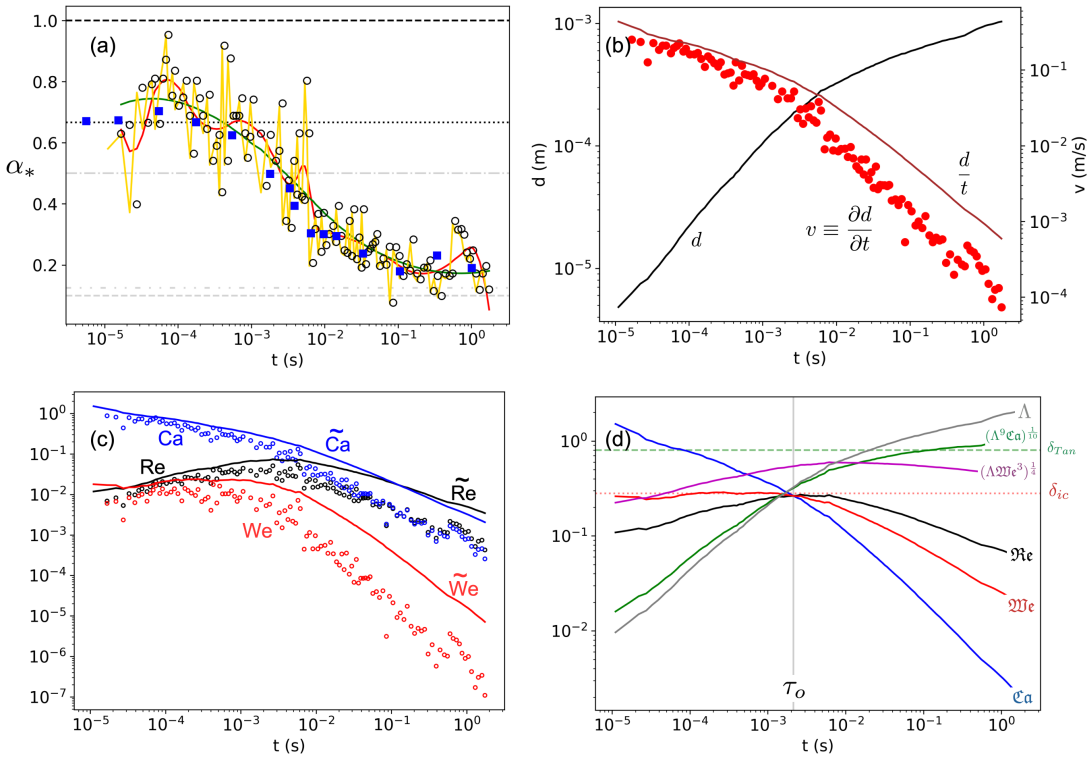

FIG. 8: Alternative dimensionless representations for the data set 'Eddi2013 Fig6 220' [4]. (a) Apparent scaling exponent α_* obtained using different methods: difference between adjacent points on logarithmic scale (open circles), logarithmic derivative after cubic interpolations of the data points obtained with the method interpolate.splprep on python with two different smoothing parameters (red and green), by computing the ratio vt/d (yellow), and as provided in the original article [4] (blue squares). (b) Comparison between the speed $v \equiv \partial d/\partial t$ (red dots) and the speed d/t (dark red line). The black curve is $d(t)$. (c) Comparison between the traditional dimensionless numbers Re, Ca and We (open circles), and the alternate numbers $\tilde{\text{Re}}$, $\tilde{\text{Ca}}$ and $\tilde{\text{We}}$. (d) Evolution of the values of the dimensionless numbers based directly on the form of the scaling laws. The numbers $\mathfrak{Re}$, $\mathfrak{Ca}$ and $\mathfrak{We}$ are identical for $t = \tau_o$. The constants δ_{ic} and δ_{Tan} identify plateaus in the evolution of $\mathfrak{We}$ and $(\Lambda^9 \mathfrak{Ca})^{\frac{1}{10}}$.

The derivation of the data $d(t)$ involved in the computation of the speed v usually introduces a source of error. To circumvent this issue, one may define alternate simple dimensionless numbers based on d and t only:

$$\tilde{\text{Re}} \equiv \frac{\rho d^2}{\eta t} = \frac{\text{Re}}{\alpha_*} \tag{25}$$

$$\tilde{\text{Ca}} \equiv \frac{\eta d}{\Gamma t} = \frac{\text{Ca}}{\alpha_*} \tag{26}$$

$$\tilde{\text{We}} \equiv \frac{\rho d^3}{\Gamma t^2} = \frac{\text{We}}{\alpha_*^2} \tag{27}$$

The values of these alternate numbers are given in SI-Fig. 8c.

As mentioned in the article, dimensionless numbers are defined modulo an overall power. Usually, this power is chosen such that the material parameters appearing in the number have integer exponents. This historical habit may not be best suited to our purpose. In the context of a comparative study of multiple scaling regimes, it may be more

judicious to define alternate numbers based directly on the form of the scaling laws:

$$\mathfrak{Re} \equiv d\Big(\frac{\rho}{\eta t}\Big)^{\frac{1}{2}} = \tilde{\mathrm{Re}}^{\frac{1}{2}} = \Big(\frac{\mathrm{Re}}{\alpha_*}\Big)^{\frac{1}{2}} \tag{28}$$

$$\mathfrak{Ca} \equiv d\frac{\eta}{\Gamma t} = \tilde{\mathrm{Ca}} = \frac{\mathrm{Ca}}{\alpha_*} \tag{29}$$

$$\mathfrak{We} \equiv d\Big(\frac{\rho}{\Gamma t^2}\Big)^{\frac{1}{3}} = \tilde{\mathrm{We}}^{\frac{1}{3}} = \frac{\mathrm{We}^{\frac{1}{3}}}{\alpha_*^{\frac{2}{3}}} \tag{30}$$

The values of these alternate numbers are given in SI-Fig. 8d.

The three simple dimensionless numbers are related by the 'we care' identity, which can be expressed in a few ways:

$$\mathrm{We} = \mathrm{CaRe} \tag{31}$$

$$\tilde{\mathrm{We}} = \tilde{\mathrm{Ca}}\tilde{\mathrm{Re}} \tag{32}$$

$$\mathfrak{We}^3 = \mathfrak{Ca}\mathfrak{Re}^2 \tag{33}$$

$$\kappa = c\nu \tag{34}$$

C. Variable geometric ratio

In addition to Re, Ca and We, we also introduced a dynamic geometric size ratio:

$$\Lambda \equiv \frac{d}{D} \tag{35}$$

For a given experiment, the value of this number evolves as the spreading, coalescence or pinching proceeds. The size ratio can be connected to a number of shape descriptors. Taken spreading as an example, the size ratio can be related to the apparent contact angle or the curvature. The actual relationship between these geometric measures and the size ratio can vary depending on context, but a few examples can help as an illustration.

If the spreading geometry follows a pancake with cylindrical symmetry, then conservation of volume imposes that $D^3 \propto hd^2$, where h is the height of the pancake. The size ratio of the pancake is then $h/d \propto \Lambda^{-3}$.

If the spreading follows a spherical cap geometry, then the conservation of volume is expressed as $D^3 \propto \theta d^3$, where $\theta \propto \Lambda^{-3}$ is the apparent contact angle.

D. Dimensionless constants

In the article, we introduced five dimensionless constants: δ_{vi}, δ_{vc}, δ_{ic}, δ_{Tan} and δ_{Ray}. Let us first discuss the three constants based on simple scaling laws associated with Re, Ca and We. The constants δ_{vi}, δ_{vc}, δ_{ic} can be understood as special values of the dynamical numbers Re, Ca and We. How these special values are defined is somewhat arbitrary, but usually one seeks time intervals where the dynamical numbers are constant and 'close to 1'. Using the traditional or alternate simple dynamical numbers, the three simple scaling laws can be expressed as:

$$d = \delta_{vi}\Big(\frac{\eta}{\rho}\Big)^{\frac{1}{2}} t^{\frac{1}{2}} \leftrightarrow \delta_{vi} = \mathfrak{Re} = \tilde{\mathrm{Re}}^{\frac{1}{2}} = \Big(\frac{\mathrm{Re}}{\alpha_*}\Big)^{\frac{1}{2}} \tag{36}$$

$$d = \delta_{vc}\frac{\Gamma}{\eta}t \leftrightarrow \delta_{vc} = \mathfrak{Ca} = \tilde{\mathrm{Ca}} = \frac{\mathrm{Ca}}{\alpha_*} \tag{37}$$

$$d = \delta_{ic}\Big(\frac{\Gamma}{\rho}\Big)^{\frac{1}{3}} t^{\frac{2}{3}} \leftrightarrow \delta_{ic} = \mathfrak{We} = \tilde{\mathrm{We}}^{\frac{1}{3}} = \frac{\mathrm{We}^{\frac{1}{3}}}{\alpha_*^{\frac{2}{3}}} \tag{38}$$

The numbers δ_{vi}, δ_{vc} and δ_{ic} are understood as constant, which are meant to identify the values of plateaus exhibited by the time-series $\mathfrak{Re}(t)$,$\mathfrak{Ca}(t)$ and $\mathfrak{We}(t)$. Thus, in the following we will use the symbols $\mathfrak{Re}_0$,$\mathfrak{Ca}_0$ and $\mathfrak{We}_0$ to respectively stand for δ_{vi}, δ_{vc} and δ_{ic}. For instance, in SI-Fig. 8d, we can identify a roughly constant value of $\mathfrak{We}$ for 10^{-5} s $\lesssim t \lesssim 2\ 10^{-3}$ s, giving $\delta_{ic} = \mathfrak{We}_0 \simeq 0.28$. Then, as stated in the article, the special value of the traditional Weber number is $\mathrm{We}_0 = \mathfrak{We}_0^3\alpha_0^2$, with $\alpha_0 = \frac{2}{3}$.

In contrast to the three simple scaling laws, the two-size dependent regimes discussed in the article cannot be derived by simple dimensional analysis. In simple scaling laws, the length d depends on three quantities, the variable

t and a choice of two material parameters. In contrast, the size-dependent regimes also depend on D, which does not lead to a unique possible scaling. When expressed in terms of dimensionless numbers, the size-dependent regimes are connected to products between simple dynamical numbers and the size ratio:

$$d = \delta_{Tan}\Big(\frac{\Gamma}{\eta}\Big)^{\frac{1}{10}} D^{\frac{9}{10}} t^{\frac{1}{10}} \leftrightarrow \delta_{Tan} = (\Lambda^9 \mathfrak{Ca})^{\frac{1}{10}} = (\Lambda^9 \tilde{\mathrm{Ca}})^{\frac{1}{10}} = \Big(\Lambda^9 \frac{\mathrm{Ca}}{\alpha_*}\Big)^{\frac{1}{10}} \tag{39}$$

$$d = \delta_{Ray}\Big(\frac{\Gamma D}{\rho}\Big)^{\frac{1}{4}} t^{\frac{1}{2}} \leftrightarrow \delta_{Ray} = (\Lambda \mathfrak{We}^3)^{\frac{1}{4}} = (\Lambda \tilde{\mathrm{We}})^{\frac{1}{4}} = \Big(\Lambda \frac{\mathrm{We}}{\alpha_*^2}\Big)^{\frac{1}{4}} \tag{40}$$

The curves corresponding to $(\Lambda^9 \tilde{\mathrm{Ca}})^{\frac{1}{10}}$ and $(\Lambda \tilde{\mathrm{We}})^{\frac{1}{4}}$ are given in SI-Fig. 8d, on which we indicate the value of δ_{Tan} corresponding to a plateau of $(\Lambda^9 \tilde{\mathrm{Ca}})^{\frac{1}{10}}$. Note that this plateau is rather limited due to the effect of gravity, which brings α closer to $\frac{1}{8}$ rather than $\frac{1}{10}$ [5].

In practice, the values of the dimensionless constants used in the article were obtained by directly fitting the data $d(t)$ to a particular exponent in a prescribe time range, and are most often equal to the values provided in the original papers. See section III I for a discussion on a fitting procedure letting the exponent free to adopt values beyond the fives regimes discussed in the article.

E. Ohnesorge and Laplace numbers

In contrast to the three simple dimensionless numbers, the Ohnesorge number depends on three rather than two material parameters. In addition, like the size ratio, the Ohnesorge number depends on the extrinsic size D. As stated in the article, the Ohnesorge number can be expressed from the simple dimensionless numbers as:

$$\mathrm{Oh}^2 \equiv \frac{\eta^2}{\Gamma \rho D} = \frac{\mathrm{Ca}}{\mathrm{Re}}\Lambda = \frac{\mathrm{We}}{\mathrm{Re}^2}\Lambda = \frac{\mathrm{Ca}^2}{\mathrm{We}}\Lambda \tag{41}$$

The different decompositions are built in such a way that the product is independent of the variables d and t. Thus, the Ohnesorge number is a constant in each experiment.

The Ohnesorge number can also be written in terms of the kinematic ratios associated with the material parameters:

$$\mathrm{Oh} = \frac{\nu}{(\kappa D)^{\frac{1}{2}}} = \Big(\frac{\nu}{cD}\Big)^{\frac{1}{2}} = \frac{\kappa^{\frac{1}{2}}}{cD^{\frac{1}{2}}} \tag{42}$$

where we recall that $\nu \equiv \eta/\rho$, $\kappa \equiv \Gamma/\rho$ and $c \equiv \Gamma/\eta$.

The Laplace number $\mathrm{La} = \mathrm{Oh}^{-2}$ gives an alternative definition of the dimensionless combination present in the Ohnesorge number. Again, dimensionless numbers are defined modulo an overall power.

F. Dimensionless lengths

Of the four systems of units discussed in the article, three share the same dimensionless length, which is none other than the size ratio:

$$\frac{d}{\ell_{vi}} = \frac{d}{\ell_{vc}} = \frac{d}{\ell_{ic}} = \frac{d}{D} = \Lambda \tag{43}$$

In contrast, the dimensionless length of the Ohnesorge units compares the variable d to the intrinsic Ohnesorge length ℓ_o, which can be expressed from D by using the Ohnesorge number:

$$\frac{d}{\ell_o} = \frac{d}{D}\frac{D}{\ell_o} = \Lambda \mathrm{La} = \frac{\Lambda}{\mathrm{Oh}^2} = \frac{\mathrm{Re}}{\mathrm{Ca}} = \frac{\mathrm{Re}^2}{\mathrm{We}} = \frac{\mathrm{We}}{\mathrm{Ca}^2} \tag{44}$$

G. Dimensionless times

In the article, we used four different time scales related by the Ohnesorge number:

$$\tau_{vi} \xrightarrow{\times \mathrm{Oh}} \tau_{ic} \xrightarrow{\times \mathrm{Oh}} \tau_{vc} \xrightarrow{\times \mathrm{Oh}^2} \tau_o \tag{45}$$

$$\frac{\rho D^2}{\eta} \xrightarrow{\times \mathrm{Oh}} \Big(\frac{\rho D^3}{\Gamma}\Big)^{\frac{1}{2}} \xrightarrow{\times \mathrm{Oh}} \frac{\eta D}{\Gamma} \xrightarrow{\times \mathrm{Oh}^2} \frac{\eta^3}{\Gamma^2 \rho} \tag{46}$$

Using these time scales in conjunction with the variable t, we built four dimensionless times that can be expressed from the simple dimensionless numbers. The three size-dependent time scales can be obtained from the associated simple dimensionless numbers as follows:

$$\frac{t}{\tau_{vi}} = \Big(\frac{\Lambda}{\mathfrak{Re}}\Big)^2 = \frac{\Lambda^2}{\tilde{\mathrm{Re}}} = \alpha_* \frac{\Lambda^2}{\mathrm{Re}} \tag{47}$$

$$\frac{t}{\tau_{ic}} = \Big(\frac{\Lambda}{\mathfrak{We}}\Big)^{\frac{3}{2}} = \frac{\Lambda^{\frac{3}{2}}}{\tilde{\mathrm{We}}^{\frac{1}{2}}} = \alpha_* \frac{\Lambda^{\frac{3}{2}}}{\mathrm{We}^{\frac{1}{2}}} \tag{48}$$

$$\frac{t}{\tau_{vc}} = \frac{\Lambda}{\mathfrak{Ca}} = \frac{\Lambda}{\tilde{\mathrm{Ca}}} = \alpha_* \frac{\Lambda}{\mathrm{Ca}} \tag{49}$$

Note that the ratios $\frac{\Lambda}{\mathfrak{Re}}$, $\frac{\Lambda}{\mathfrak{We}}$ and $\frac{\Lambda}{\mathfrak{Ca}}$ effectively produce inverse dimensionless numbers where the varying length scale d has been replaced by the constant D, such that the only variability in the ratios come from t.

The fourth dimensionless time can be expressed in a few equivalent ways illustrating different properties:

$$\frac{t}{\tau_o} \equiv \frac{t\Gamma^2\rho}{\eta^3} = \frac{\Lambda}{\tilde{\mathrm{Ca}}\mathrm{Oh}^2} = \frac{1}{\mathfrak{Ca}}\frac{d}{\ell_o} = \alpha_* \frac{\mathrm{Re}}{\mathrm{Ca}^2} = \alpha_* \frac{\mathrm{We}}{\mathrm{Ca}^3} = \alpha_* \frac{\mathrm{Re}^2}{\mathrm{WeCa}} \tag{50}$$

In Ohnesorge's units the alternate dimensionless numbers can be understood as the dimensionless equivalents of the kinematic quantities c, $\nu^{\frac{1}{2}}$ and $\kappa^{\frac{1}{3}}$, which are now understood as variable rather than constant:

$$\frac{d}{\ell_o} = \mathfrak{Ca}(t)\frac{t}{\tau_o} = \mathfrak{Re}(t)\Big(\frac{t}{\tau_o}\Big)^{\frac{1}{2}} = \mathfrak{We}(t)\Big(\frac{t}{\tau_o}\Big)^{\frac{2}{3}} \tag{51}$$

This polymorphism of the Ohnesorge units is exhibited quite visually by the intersections of the three curves $\mathfrak{Re}(t)$, $\mathfrak{Ca}(t)$ and $\mathfrak{We}(t)$, marking the instant with $t = \tau_o$, as shown on an example in SI-Fig. 8d.

H. Dimensionless unit prefactors

In sections II E and II F we described how the actual units used in the article include prefactors taking into account the dimensionless constants. For instance, in the case of dynamics decomposed into an early visco-capillary regime and a late inertio-capillary regime, then $\gamma_1 = (\delta_{ic}/\delta_{vc})^3$ and $\gamma_2 = \delta_{vc}(\delta_{ic}/\delta_{vc})^3$. Putting everything together and choosing the Ohnesorge units as an example, one has:

$$\frac{d}{\ell_o^*} = \mathcal{C}\frac{t}{\tau_o^*} = \mathcal{R}\Big(\frac{t}{\tau_o^*}\Big)^{\frac{1}{2}} = \mathcal{W}\Big(\frac{t}{\tau_o^*}\Big)^{\frac{2}{3}} \tag{52}$$

where we have defined renormalized versions of the simple dimensionless numbers:

$$\mathcal{C} \equiv \frac{\mathfrak{Ca}(t)}{\mathfrak{Ca}_0} \tag{53}$$

$$\mathcal{R} \equiv \frac{\mathfrak{Re}(t)}{\mathfrak{Re}_0} \tag{54}$$

$$\mathcal{W} \equiv \frac{\mathfrak{We}(t)}{\mathfrak{We}_0} \tag{55}$$

With these new definitions, we have $\mathcal{W}^3 = \mathcal{C}\mathcal{R}^2$.

Overall, the dimensionless plots in the four systems of units provided in the article can be understood as representations of choices of different ratios of the simple dimensionless numbers normalized by their constant values. This mapping from dimensionless time and space to simple dimensionless numbers can be illustrated in Ohnesorge units, where the various sectors of the plot are associated with different inequalities between the dimensionless numbers, as illustrate in SI-Fig. 9.

I. Quasi-properties and generalized dynamical number

So far we have assumed that the five scaling laws described in the article provided a good description of most of the regimes encountered in the analyzed experiments on spreading, coalescence and pinching. Indeed, the various

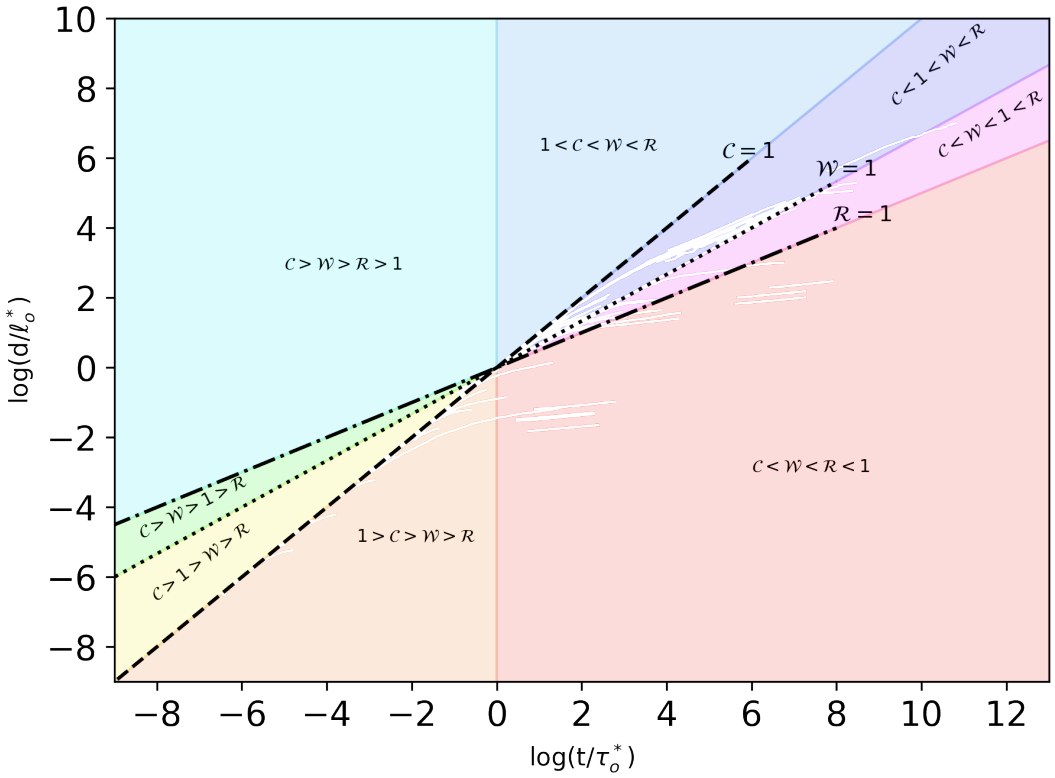

FIG. 9: The different dynamical domains in Ohnesorge units. Each colored domain corresponds to a different inequality between the three simple dimensionless numbers and the threshold 1. Note that because of the 'we care' relationship, *i.e.* $\mathcal{W}^3 = \mathcal{C}\mathcal{R}^2$, the only two possible inequalities between the three simple dimensionless numbers are $\mathcal{C} < \mathcal{W} < \mathcal{R}$ (if $t > \tau_o$) or $\mathcal{C} > \mathcal{W} > \mathcal{R}$ (if $t < \tau_o$). The different domains are then defined by the placement of 1 within these inequalities.

representations of the data in the four systems of units largely supported this hypothesis. Although close to the reference exponents provided by the five scalings, the actual values may be slightly different. For instance, data may display an exponent $\alpha \simeq 0.45$ instead of $\alpha = \frac{1}{2}$ for Rayleigh's law. The dimensionless constants δ_{vc}, δ_{ic} etc. provided in Tables VII-IX were all obtained by assuming one of the standard exponents and fitting the experimental data with the associated regime. Instead, we can relax the constraint on the value of the exponent and fit the data to obtain both the exponent and the prefactor.

If $d = Kt^\alpha$, dimensional analysis imposes that $[K] = \mathcal{L}.\mathcal{T}^{-\alpha}$. We know that if α is a rational number constructed from small integers, then the kinematic coefficient K can be connected to ratios of traditional material parameters, like Γ/η, $(\Gamma/\rho)^{\frac{1}{3}}$ etc. If the value of α cannot be expressed as a simple fraction, one may say that K is a 'quasi-property' [6]. In this case, the different systems of units can still be used to estimate an expected value of K. For instance, if one assumes than a spreading regime fitted by $d = Kt^\alpha$ can be well represented by the Ohnesorge units, then the expected value of K is $K_o = \ell_o.\tau_o^{-\alpha}$, irrespective of the value of α, *i.e.* even if it is beyond 1, $\frac{1}{2}$ or $\frac{2}{3}$. For any particular system of units with length ℓ and time τ, one can define a generalized dynamical dimensionless number:

$$\mathfrak{N}(\alpha) \equiv \frac{dt^{-\alpha}}{\ell\tau^{-\alpha}} \tag{56}$$

For instance, for the Ohnesorge units we have:

$$\mathfrak{N}_o(\alpha) \equiv \frac{d\Gamma^{1-2\alpha}\rho^{1-\alpha}}{\eta^{2-3\alpha}t^\alpha} = \begin{cases} \mathfrak{C} & \text{if } \alpha = 1 \\ \mathfrak{W} & \text{if } \alpha = \frac{2}{3} \\ \mathfrak{R} & \text{if } \alpha = \frac{1}{2} \end{cases} \tag{57}$$

The values of $\mathfrak{N}_o$ and α obtained by fitting both the prefactor and the exponent on all the regimes of the data shown in the article are given in SI-Fig. 10. Regimes exhibiting a value of $\mathfrak{N}_o$ close to 1 are in good agreement with

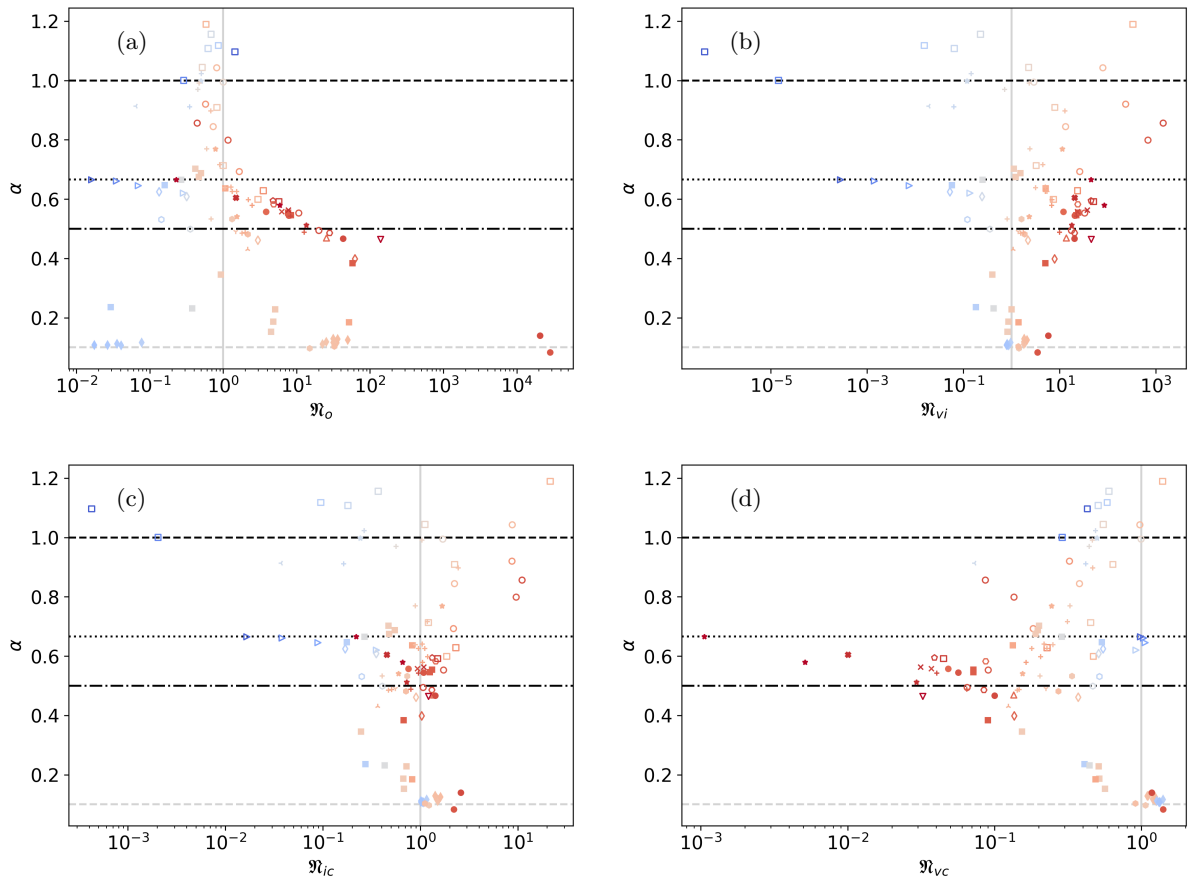

FIG. 10: Spreading exponent and generalized dynamical dimensionless numbers in Ohnesorge, visco-inertial, visco-capillary and inertio-capillary units. Agreement with a particular system of units corresponds $\mathfrak{N} \propto 1$ (vertical line).

the Ohnesorge units. In contrast, dynamics associated with very small or large values of $\mathfrak{N}_o$ indicate departure from the Ohnesorge units. This is particularly true when the extrinsic size D starts to have an impact, as in the Tanner or Rayleigh regimes. In SI-Fig. 10 we also provide plots for the values of $\mathfrak{N}_{vi}$, $\mathfrak{N}_{ic}$ and $\mathfrak{N}_{vc}$, by using the respective visco-inertial, inertio-capillary and visco-capillary units to define the $\mathfrak{N}$.

IV. OPEN QUESTIONS

In this section, we highlight some of the issues raised in the main article by providing additional plots focusing on sub-sets of the experimental data.

A. Size-dependence of the inertio-capillary regimes for Oh< 1

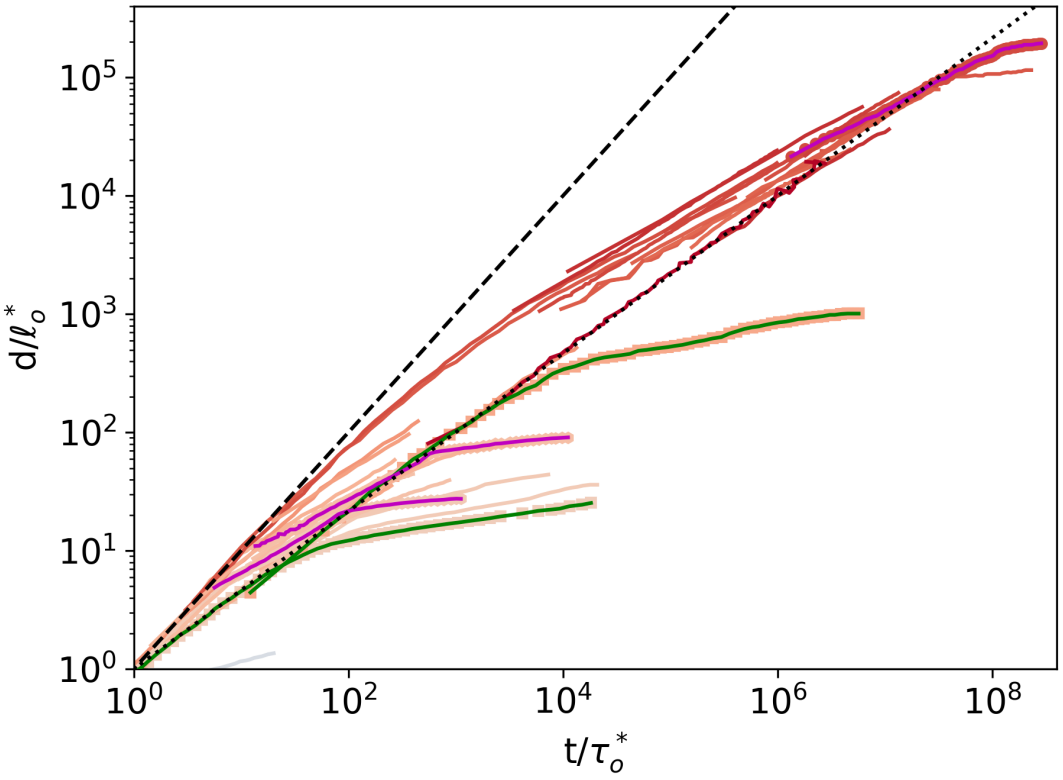

FIG. 11: Spreading, coalescence and pinching dynamics for $d/\ell_o^* > 1$ and $t/\tau_o^* > 1$. The highlighted spreading curves have Oh $= 2.31\ 10^{-1}$ ('Chen2014 Fig3b 60cP'), Oh $= 2.95\ 10^{-1}$ ('Eddi2013 Fig4 0p37'), Oh $= 5.71\ 10^{-2}$ ('Eddi2013 Fig6 11') and Oh $= 5.71\ 10^{-2}$ ('Biance2004 Fig3 1p2').

In SI-Fig. 11 we provide a close-up on the region $d/\ell_o^* > 1$ and $t/\tau_o^* > 1$. In this sector of the operating space, we have $\mathcal{C} < \mathcal{W} < \mathcal{R}$. Data from spreading, coalescence and pinching exhibit two possible trends. Starting at $d/\ell_o^* = 1$ and $t/\tau_o^* = 1$, some dynamics directly follow the inertio-capillary regime ($\alpha = \frac{2}{3}$, dotted line), while other remain on the visco-capillary regime ($\alpha = 1$, dashed line), until $d/\ell_o^* = t/\tau_o^* = \text{Oh}^{-1}$, after which they follow Rayleigh's regime ($\alpha = \frac{1}{2}$), reaching $d/\ell_o^* = D$ when crossing the dotted line. To put it bluntly: why do some dynamics take a short cut via the $\frac{2}{3}$ regime, while other take the long route through Rayleigh's regime? Let us take spreading as an example. Highlighted in SI-Fig. 11 are four spreading curves with Oh $= 2.31\ 10^{-1}$ ('Chen2014 Fig3b 60cP'), Oh $= 2.95\ 10^{-1}$ ('Eddi2013 Fig4 0p37'), Oh $= 5.71\ 10^{-2}$ ('Eddi2013 Fig6 11') and Oh $= 5.71\ 10^{-2}$ ('Biance2004 Fig3 1p2'). The data from Eddi *et al.* abide to the $\frac{2}{3}$ scaling, while the data from Chen *et al.* and Biance *et al.* follow Rayleigh's regime. Some criterion beyond the value of the Ohnesorge number seems to dictate the course of events. Note that in experiments by Chen *et al.*, the substrate was partially wetting ($\theta = 63°$).

B. Inertio-capillary regime for Oh>1

The existence of a $\frac{2}{3}$ regime of spreading for Oh<1 as exhibited above is not too surprising and has been discussed in the literature []. While compiling the data reproduced in the article, we also noticed that some spreading experiments with Oh$\gtrsim 1$ could also be interpreted as following a $\frac{2}{3}$ regime extending in the region $d/\ell_o^* < 1$ and $t/\tau_o^* < 1$, where $\mathcal{C} > 1 \gtrsim \mathcal{W} > \mathcal{R}$. These experiments are labeled 'Eddi2013 Fig6 220' and 'Eddi2013 Fig6 1120'. In the main article and in the Table VII we chose to interpret these data from a visco-capillary perspective in accordance with the original paper [4]. That is to say that the spreading was interpreted as displaying a visco-capillary regime with an intermediate regime dominated by a logarithmic correction. In this interpretation, the first few data points are used to obtain a value of δ_{vc}, and the associated unit prefactors γ_1 and γ_2 computed with the addition of the late spreading prefactor δ_{Tan} produce the curves displayed in SI-Fig. 12a. The values of δ_{vc} derived in this way are sensibly larger than the average, as can be seen in SI-Fig. 5. A different way to interpret these two data sets is to consider than the early regime abides to a $\frac{2}{3}$ regime, and to build the unit prefactors from δ_{ic} and δ_{Tan}. The example of 'Eddi2013 Fig6 220' was treated in details in SI-Fig. 8, where it was quite convincing than for $t/\tau_o^* < 1$ the dynamics displayed a constant Weber number, and so followed the $\frac{2}{3}$ regime. In SI-Fig. 12b we give the result of interpreting the data sets 'Eddi2013 Fig6 220' and 'Eddi2013 Fig6 1120' in this alternate way. From this perspective, the inferred values of δ_{ic} are consistent but seem to decrease with increasing Ohnesorge number. We expect that investigating the dynamics at yet earlier times would help deciphering the respective roles of inertia and viscosity for the onset of spreading. More broadly for values of the Ohnesorge number close to 1, we can expect a broader diversity of dynamics than reflected in the main paper. For instance, recent data on pinching near Oh $\propto 1$ suggest a variety of rich behaviors [7]. Unfortunately, the information on the values of the material parameters used in the experiments of this reference was too scarce to allow us to reproduce the plots.

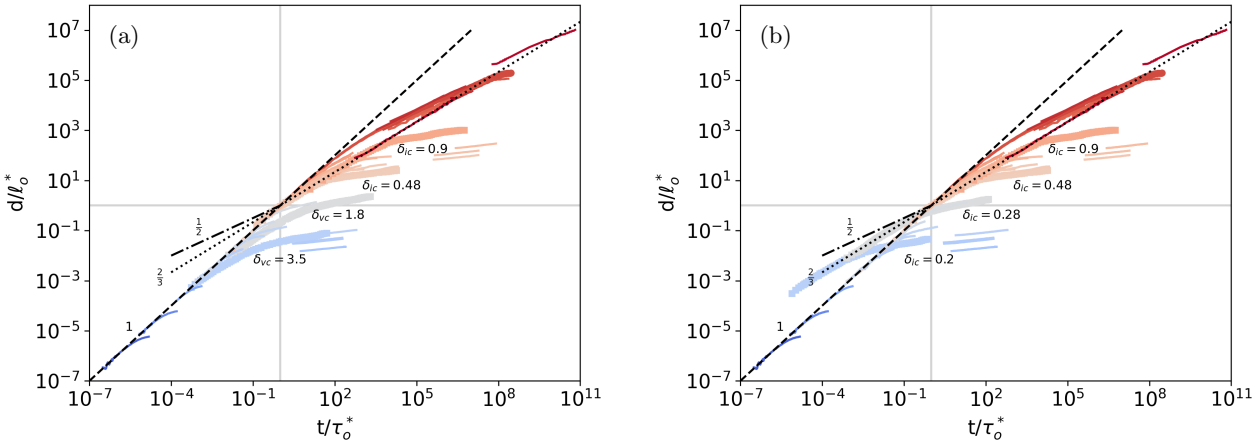

FIG. 12: Two ways to interpret the data sets 'Eddi2013 Fig6 220' (Oh = 1.1) and 'Eddi2013 Fig6 1120' (Oh = 5.6). (a) Visco-capillary interpretation: the first data points are interpreted as belonging to a visco-capillary regime, followed by a long intermediate range dominated by a logarithmic correction, finally reaching a Tanner regime in the late spreading. The fitted values of δ_{vc} and δ_{Tan} are used to compute the unit prefactors $\gamma_1 = (\delta_{Tan}/\delta_{vc})^{\frac{10}{9}}$ and $\gamma_2 = \delta_{vc}\gamma_1$. (b) Inertio-capillary interpretation: the early spreading is interpreted as an inertio-capillary regime followed by a Tanner regime in the late spreading. The fitted values of δ_{ic} and δ_{Tan} are used to compute the unit prefactors $\gamma_1 = (\delta_{Tan}/\delta_{ic})^{\frac{30}{17}}$ and $\gamma_2 = \delta_{ic}\gamma_1^{\frac{2}{3}}$.

V. ANIMATED FIGURES

The files 'Fig3_VC.gif', 'Fig3_IC.gif', 'Fig4_VI.gif' and 'Fig5_Oh.gif' give animated versions of Fig. 3, 4 and 5 of the main article, showing how every data set is included in the graph. The images used to create the animated files are given in the zip archives of the same names. Note that the values of η, ρ, Γ and D given on each image have standard units, *i.e.* Pa.s for viscosity, kg/m^3 for density, N/m for surface tension and m for the extrinsic size.

The file 'TowardOhUnits.gif' gives an animated figure built from the succession of three images with different units for the data sets shown in Fig. 5 of the main article: standard units (d in meters and t in seconds), 'bare' Ohnesorge units d/ℓ_o and t/τ_o, and normalized Ohnesorge units d/ℓ_o^* and t/τ_o^*.

VI. DETAILS ON EXPERIMENTAL DATA

In this section we provide additional details on the experiments reproduced in the article. The readers are referred to the original publications for the full context. The horizontal lines on some of the plots give the value of D, when it is within the range of the data. The vertical plain, dashed, dotted and dotted-dashed lines respectively give the values of τ_o^*, τ_{vc}^*, τ_{ic}^* and τ_{vi}^*, when within the range of the data.

Cazabat1986 Fig1a 0p78

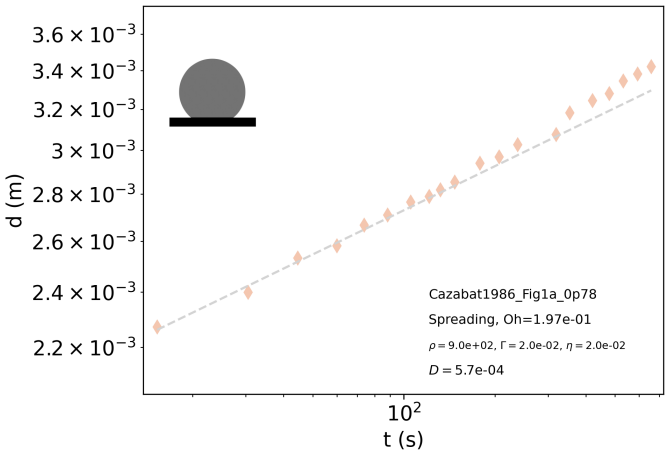

Silicone oil in ambient air, on smooth hydrophilic glass.
Effect of gravity for $d \gtrsim (\Gamma/\rho g)^{\frac{1}{2}}$.

Cazabat1986 Fig1a 1p5

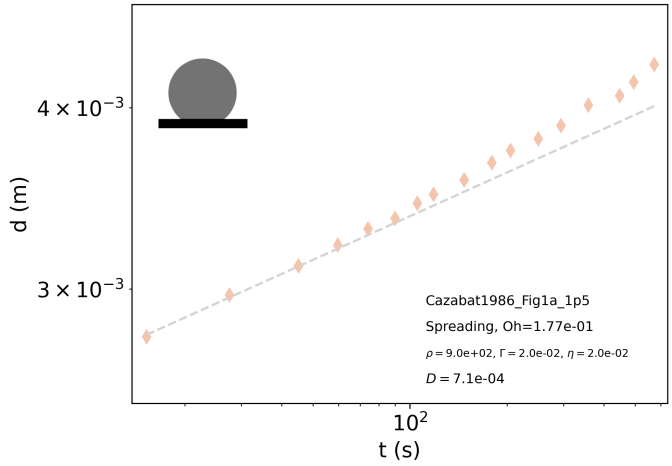

Silicone oil in ambient air, on smooth hydrophilic glass.
Effect of gravity for $d \gtrsim (\Gamma/\rho g)^{\frac{1}{2}}$.

Cazabat1986 Fig1a 2p9

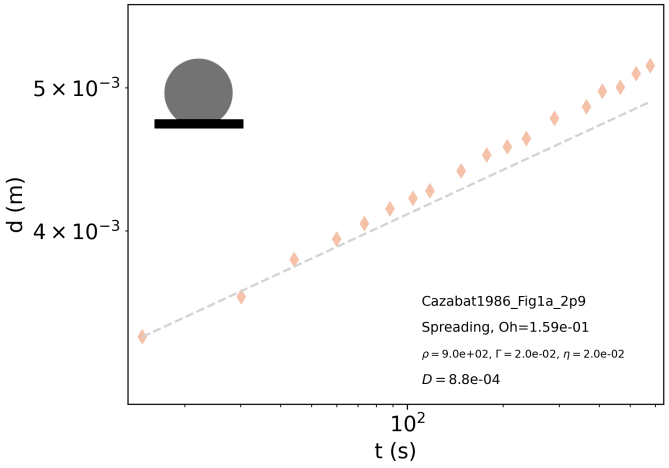

Silicone oil in ambient air, on smooth hydrophilic glass.
Effect of gravity for $d \gtrsim (\Gamma/\rho g)^{\frac{1}{2}}$.

Cazabat1986 Fig1a 3p8

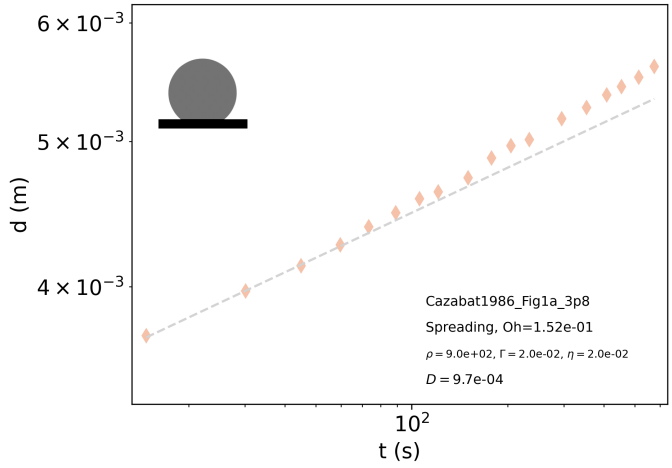

Silicone oil in ambient air, on smooth hydrophilic glass.
Effect of gravity for $d \gtrsim (\Gamma/\rho g)^{\frac{1}{2}}$.

Cazabat1986 Fig1a 4p7

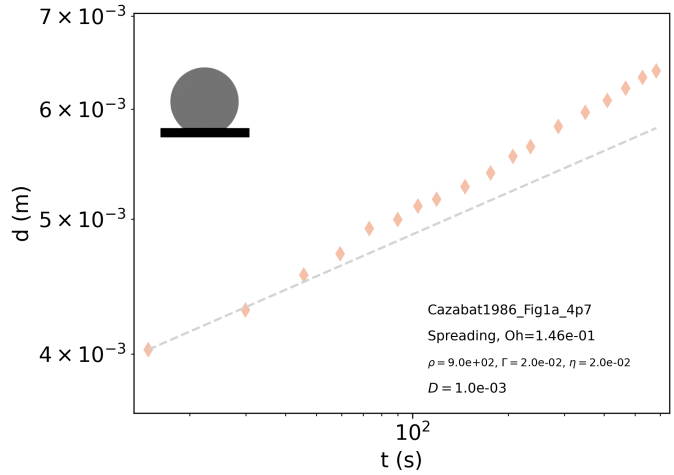

Silicone oil in ambient air, on smooth hydrophilic glass.
Effect of gravity for $d \gtrsim (\Gamma/\rho g)^{\frac{1}{2}}$.

Cazabat1986 Fig1a 7p8

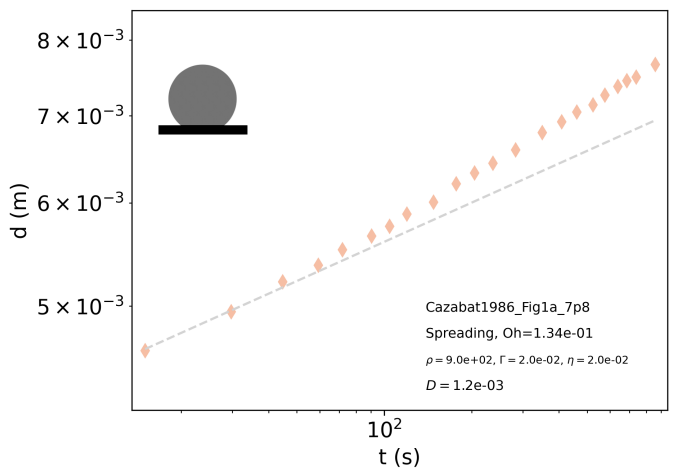

Silicone oil in ambient air, on smooth hydrophilic glass.
Effect of gravity for $d \gtrsim (\Gamma/\rho g)^{\frac{1}{2}}$.

Cazabat1986 Fig1a 14p4

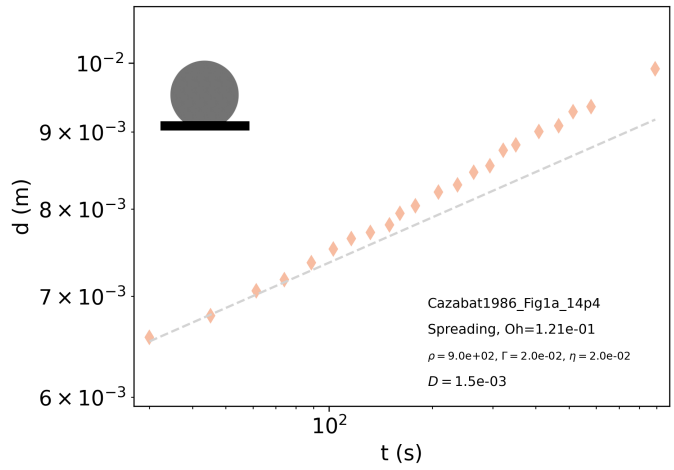

Silicone oil in ambient air, on smooth hydrophilic glass.
Effect of gravity for $d \gtrsim (\Gamma/\rho g)^{\frac{1}{2}}$.

Cazabat1986 Fig1b 37p9

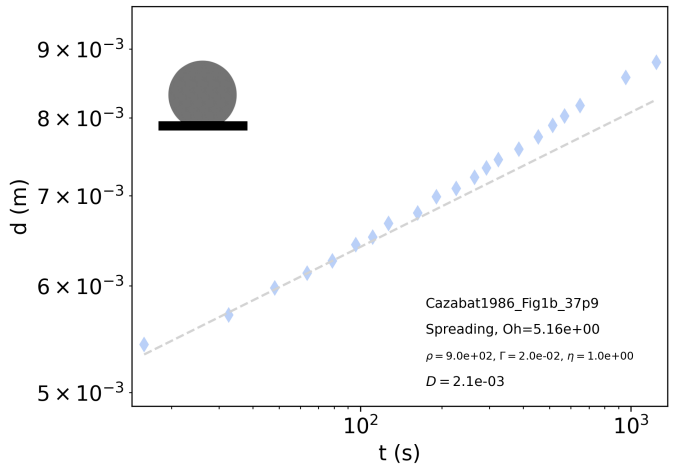

Silicone oil in ambient air, on smooth hydrophilic glass.
Effect of gravity for $d \gtrsim (\Gamma/\rho g)^{\frac{1}{2}}$.

Cazabat1986 Fig1b 5p8

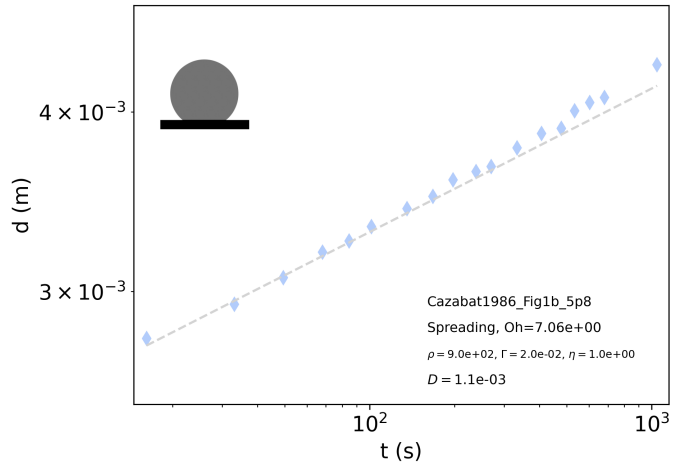

Silicone oil in ambient air, on smooth hydrophilic glass.
Effect of gravity for $d \gtrsim (\Gamma/\rho g)^{\frac{1}{2}}$.

Cazabat1986 Fig1b 4p03

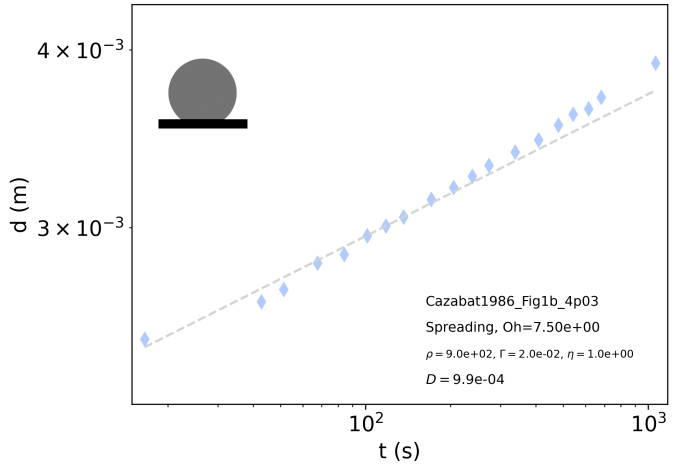

Silicone oil in ambient air, on smooth hydrophilic glass.
Effect of gravity for $d \gtrsim (\Gamma/\rho g)^{\frac{1}{2}}$.

Cazabat1986 Fig1b 1p35

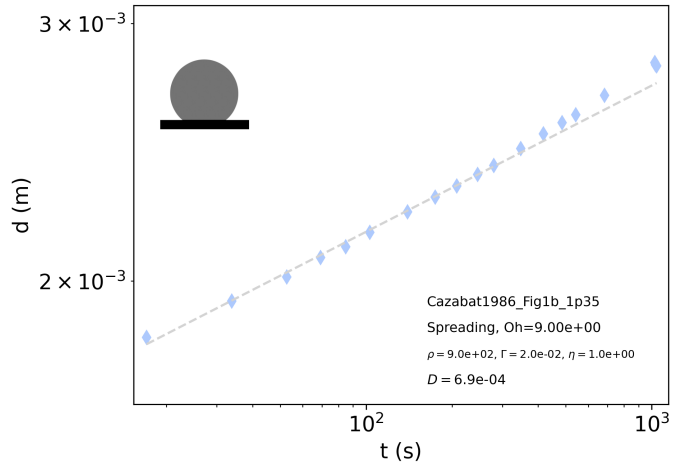

Silicone oil in ambient air, on smooth hydrophilic glass.
Effect of gravity for $d \gtrsim (\Gamma/\rho g)^{\frac{1}{2}}$.

Cazabat1986 Fig1b 0p35

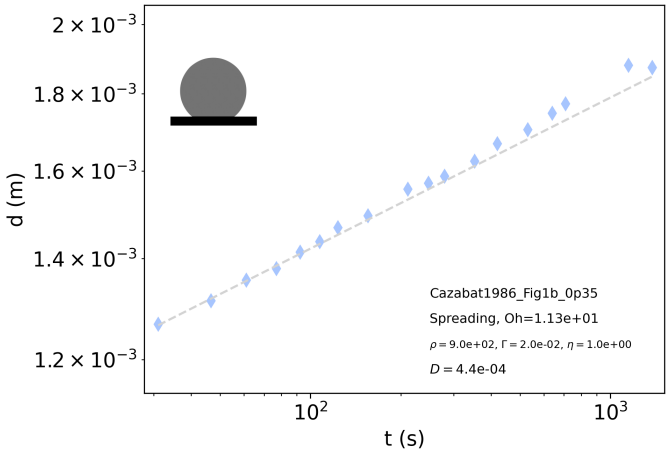

Silicone oil in ambient air, on smooth hydrophilic glass.
Effect of gravity for $d \gtrsim (\Gamma/\rho g)^{\frac{1}{2}}$.

Biance2004 Fig3 0p27

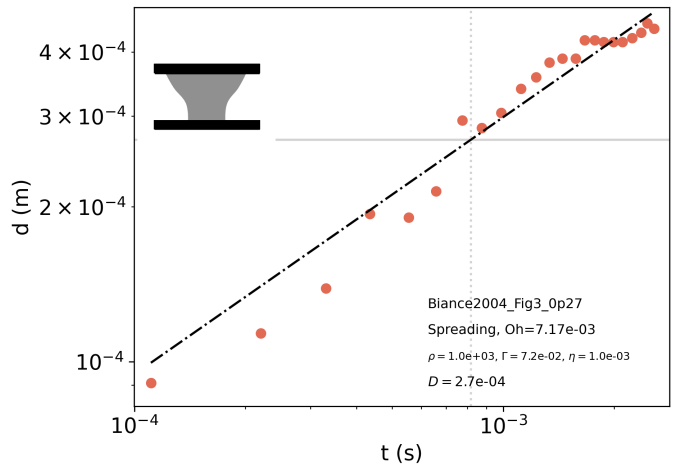

Water in ambient air, on inverted hydrophilic glass

Biance2004 Fig3 0p7

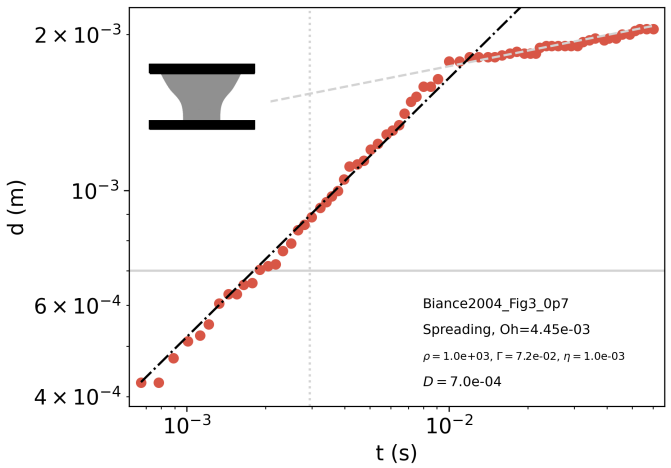

Water in ambient air, on inverted hydrophilic glass

Biance2004 Fig3 1p2

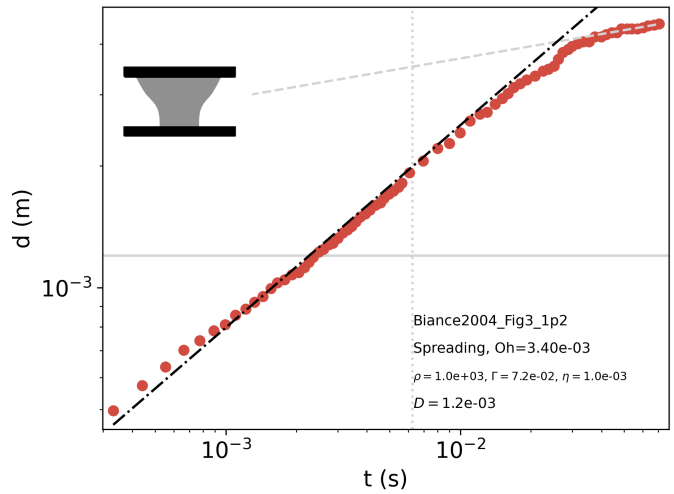

Water in ambient air, on inverted hydrophilic glass

Eddi2013 Fig4 0p37

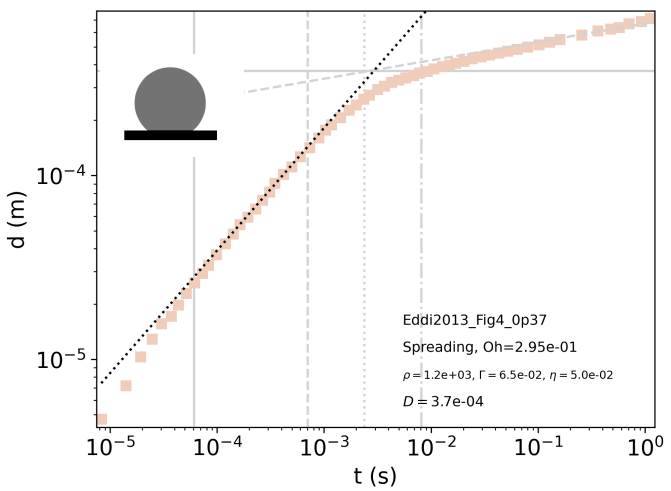

Water-glycerol mixture in ambient air, on hydrophilic glass

Eddi2013 Fig4 0p5

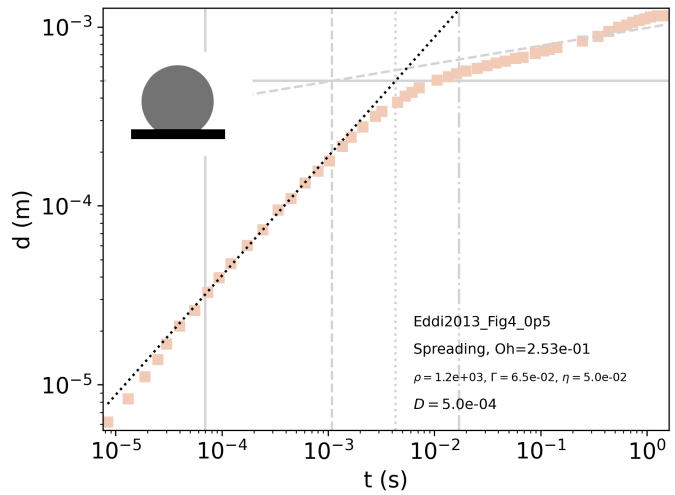

Water-glycerol mixture in ambient air, on hydrophilic glass

Eddi2013 Fig4 0p63

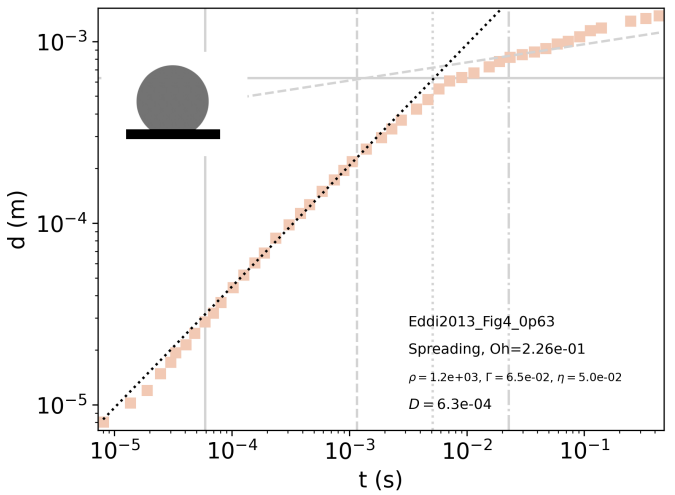

Water-glycerol mixture in ambient air, on hydrophilic glass

Eddi2013 Fig5a 105deg

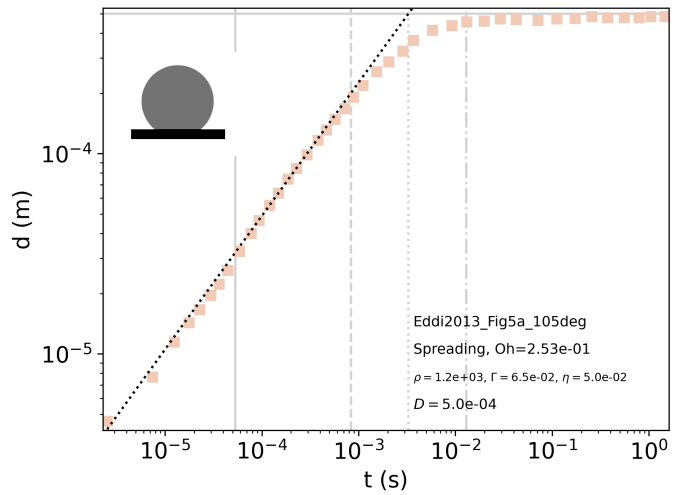

Water-glycerol mixture in ambient air,
on hydrophobic fluoropolymer-coated glass.

Eddi2013 Fig5b 0

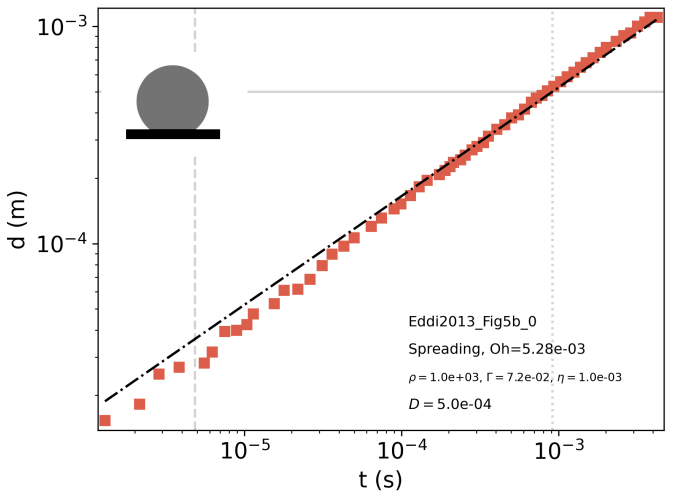

Water in ambient air, on hydrophilic glass.

Eddi2013 Fig5b 115

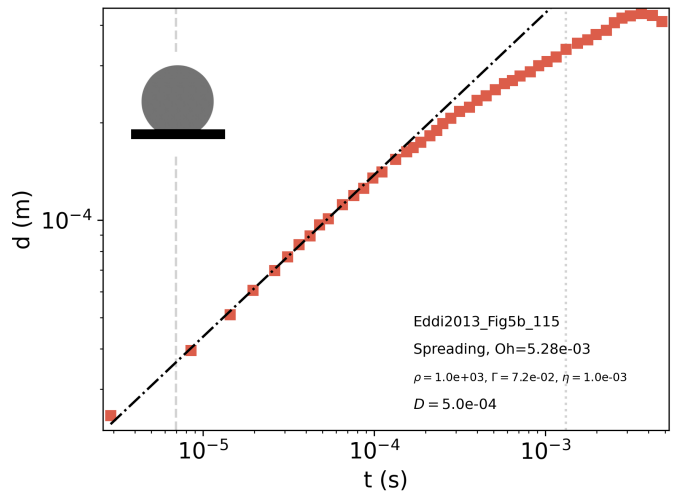

Water in ambient air, on hydrophobic Teflon-coated glass.

Eddi2013 Fig6 water

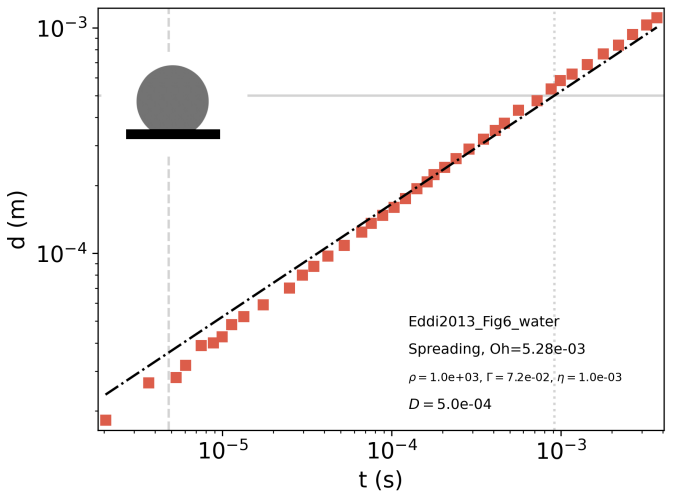

Water in ambient air, on hydrophilic glass.

Eddi2013 Fig6 11

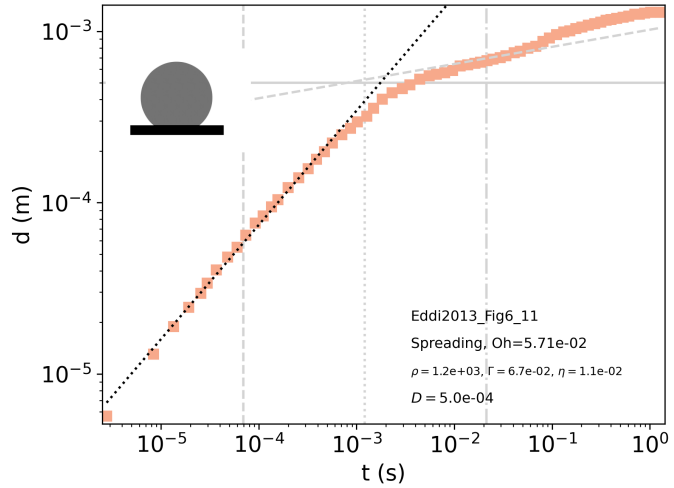

Water-glycerol mixture in ambient air, on hydrophilic glass

Eddi2013 Fig6 1120

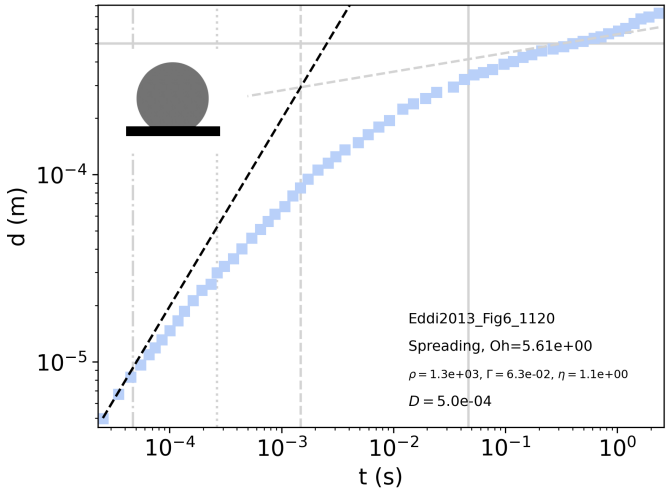

Water-glycerol mixture in ambient air, on hydrophilic glass

Eddi2013 Fig6 220

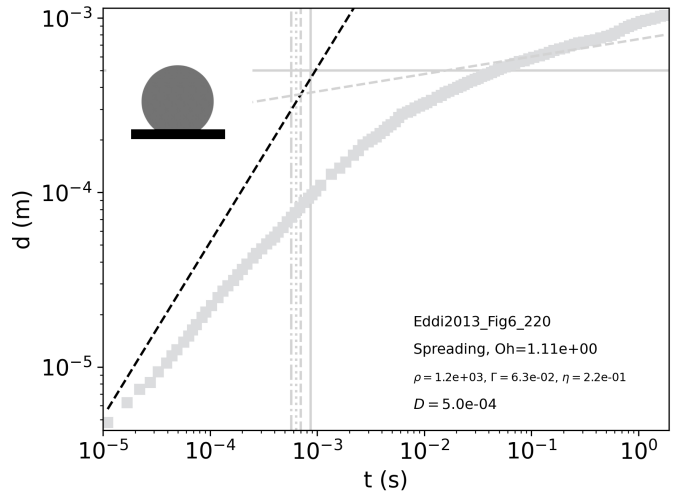

Water-glycerol mixture in ambient air, on hydrophilic glass

Chen2014 Fig3b 60cP

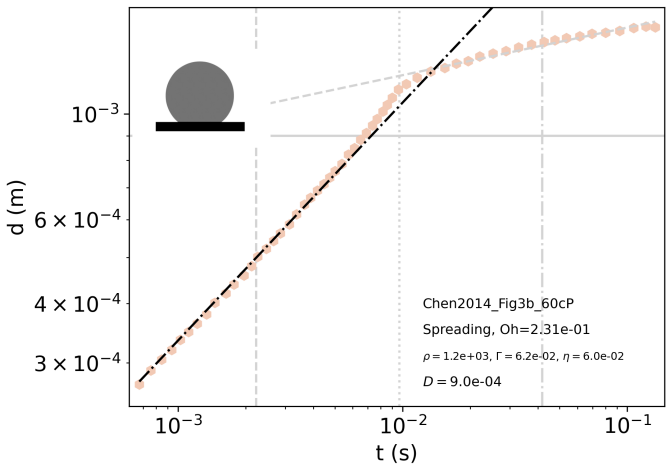

Water-glycerol mixture in ambient air, on partial wetting substrate ($\theta = 63°$).

Chen2014 Fig3b 35p5cP

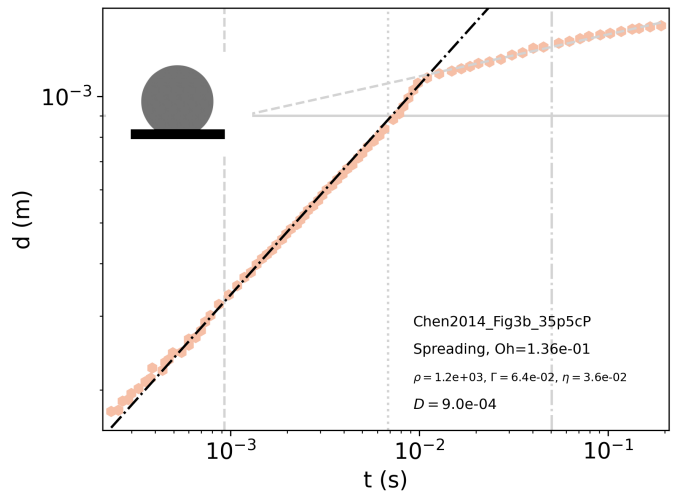

Water-glycerol mixture in ambient air, on partial wetting substrate ($\theta = 63°$).

Menchaca2001 Fig9

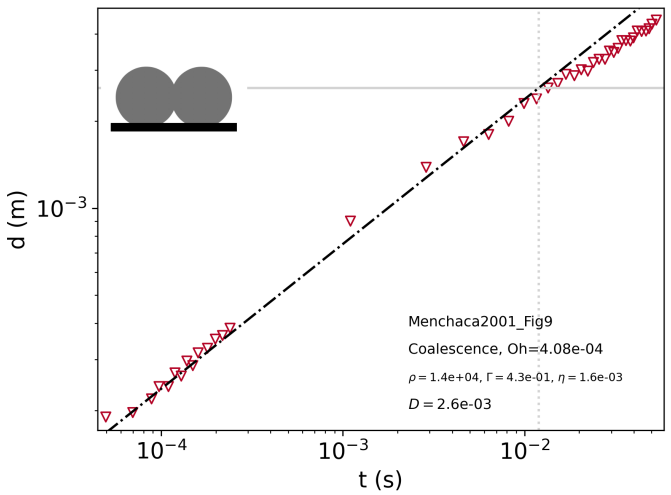

Mercury in ambient air.

Wu2004 Fig4 1p94

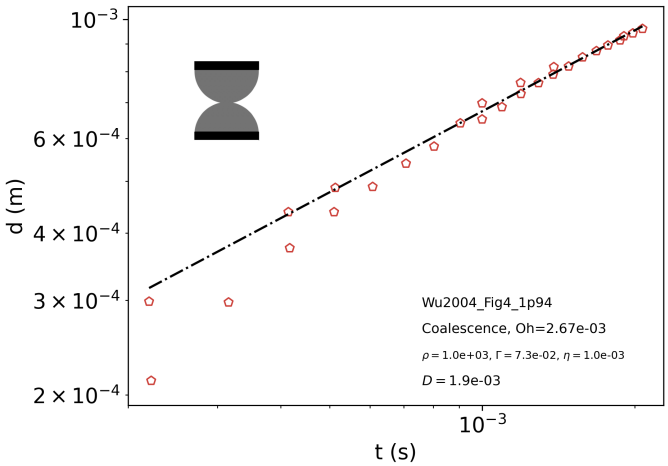

Water in ambient air.

Yao2005 100000cS 5cm

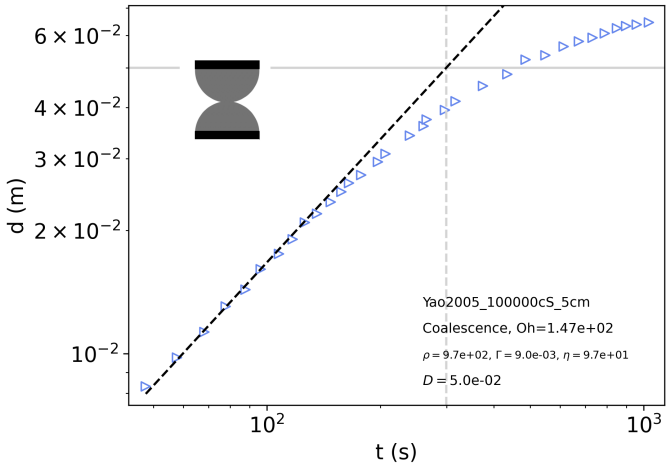

Siliconee oil in density-matched water-alcohol mixture.

Yao2005 100000cS 0p5cm

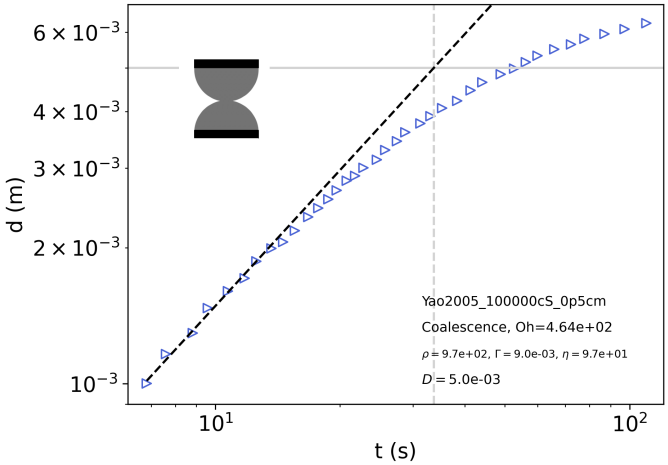

Siliconee oil in density-matched water-alcohol mixture.

Yao2005 10000cS 0p5cm

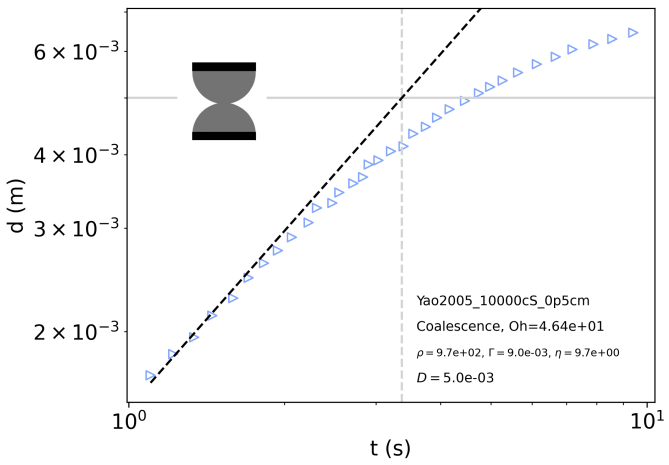

Siliconee oil in density-matched water-alcohol mixture.

Yao2005 1000cS 0p5cm

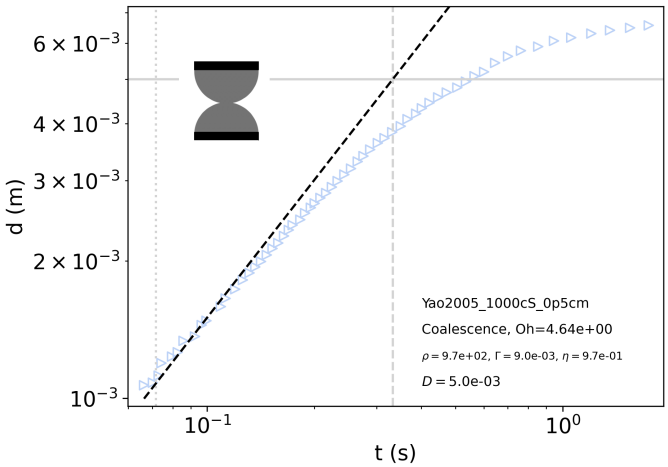

Siliconee oil in density-matched water-alcohol mixture.

Thoroddsen2005 Fig6

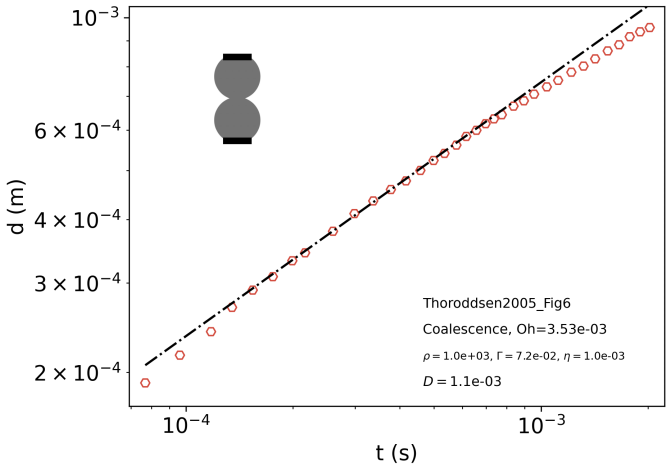

Water in ambient air.

Thoroddsen2005b Fig4

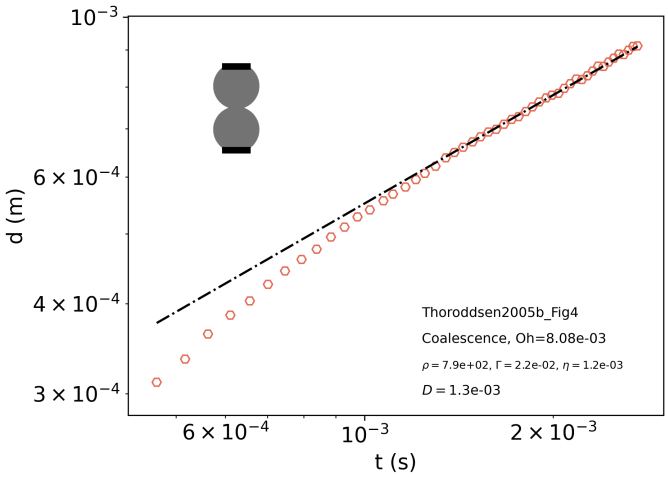

Air bubbles in ethyl alcohol.
Density and viscosity are that of the outer fluid.

Aarts2005 Fig2 100mPas

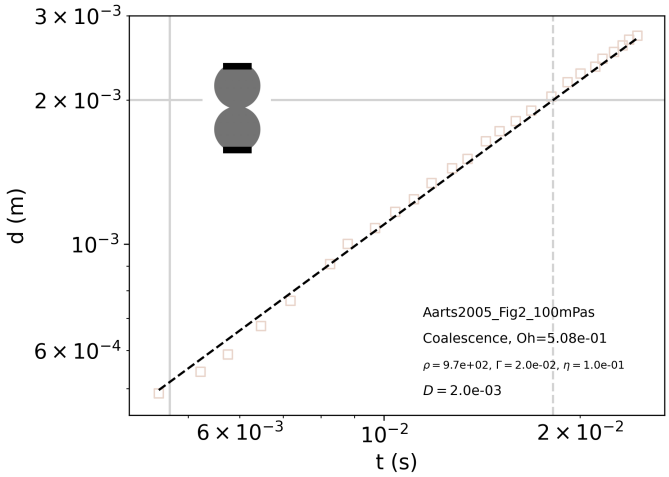

Silicone oil in ambient air.

Aarts2005 Fig2 1Pas

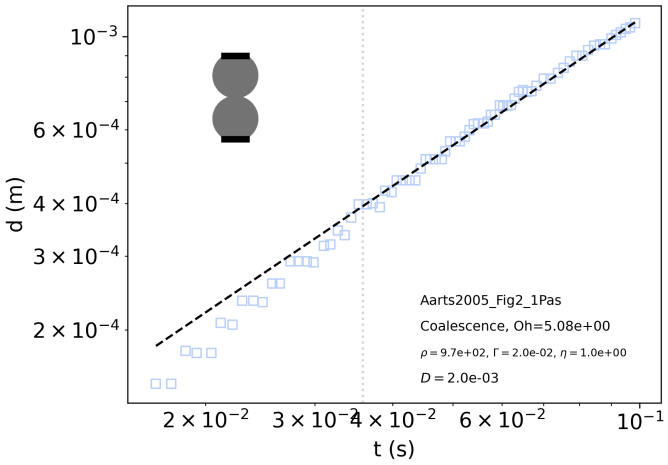

Silicone oil in ambient air.

Aarts2005 Fig2 500mPas

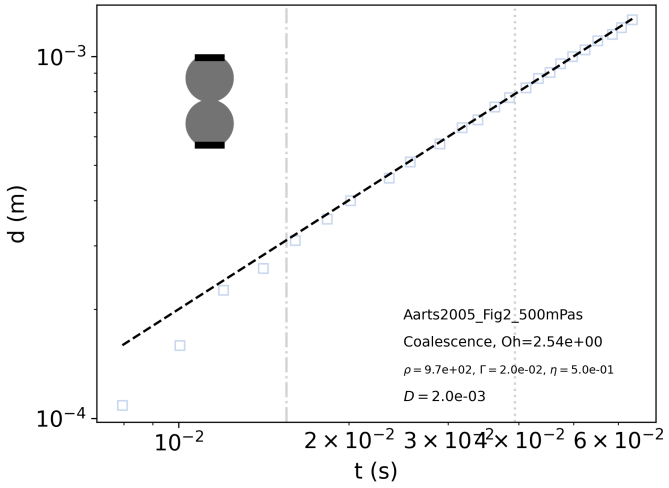

Silicone oil in ambient air.

Aarts2005 Fig2 300mPas

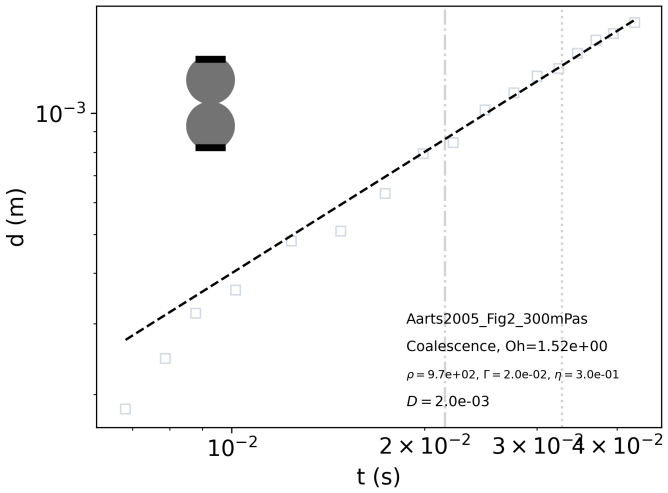

Silicone oil in ambient air.

Aarts2005 Fig3 5mPas

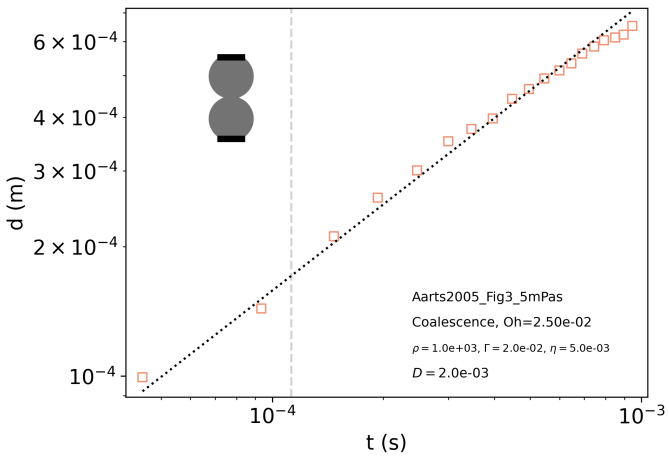

Silicone oil in ambient air.

Aarts2005 Fig3 20mPas

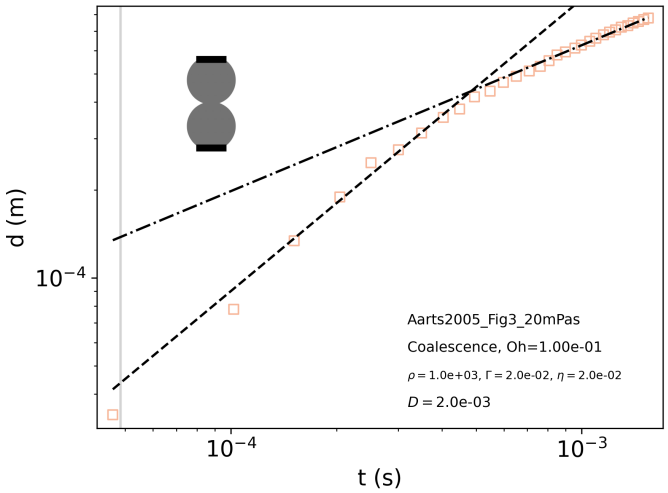

Silicone oil in ambient air.

Aarts2005 Fig3 50mPas

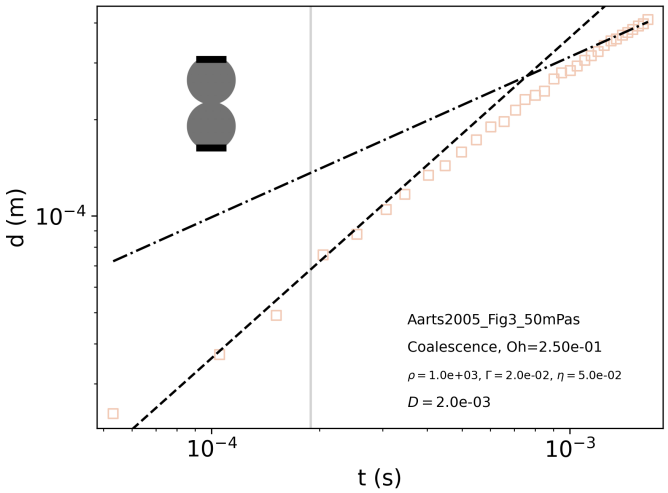

Silicone oil in ambient air.

Aarts2005 Fig3 1mPas

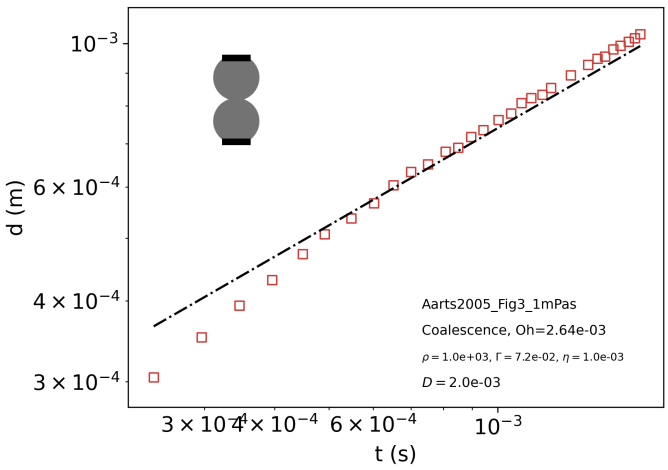

Water in ambient air.

Aarts2008 Fig9 bubb17

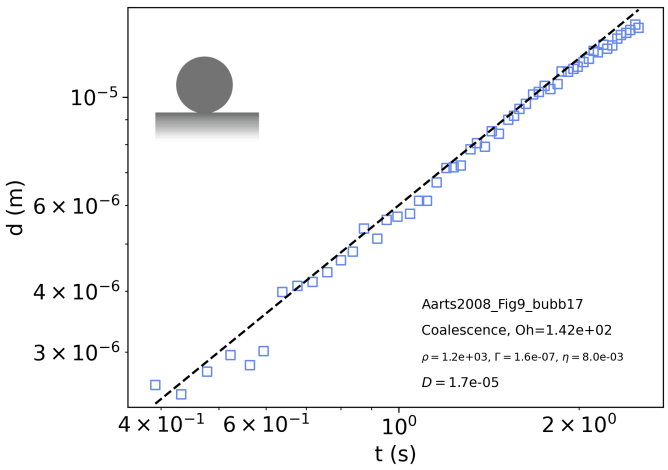

PMMA Poly(styrene) in Decalin, gas phase.
The density used is that of the PMMA colloid.

Aarts2008 Fig9 drop17

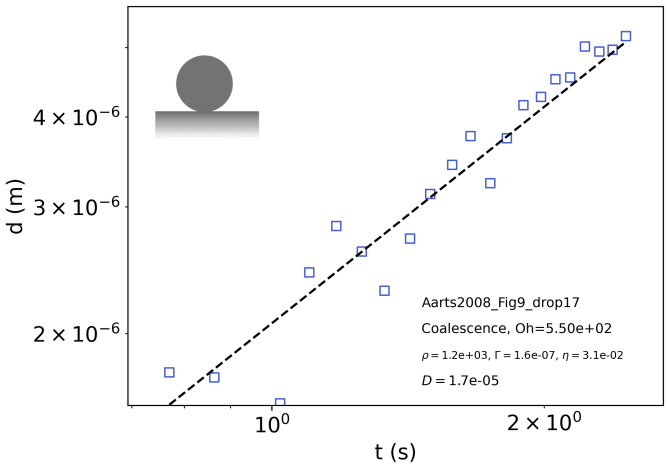

PMMA Poly(styrene) in Decalin, liquid phase.
The density used is that of the PMMA colloid.

Yokota2011 Fig2 289

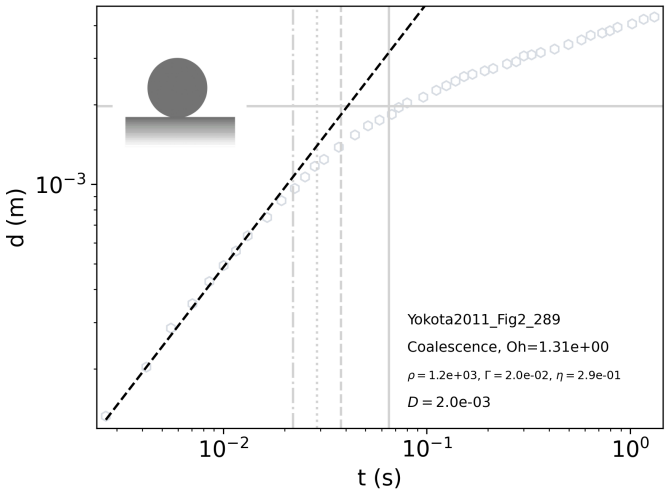

Water-glycerol mixture in PDMS oil.
A precise value of density was not available.
In a Hele-Shaw cell $D = (RH)^{\frac{1}{2}}$, where R and H are respectively the drop radius and the cell thickness.
Long-time behavior follows $d/\ell_{vc} \propto (t/\tau_{vc})^{\frac{1}{4}}$.

Yokota2011 Fig2 888

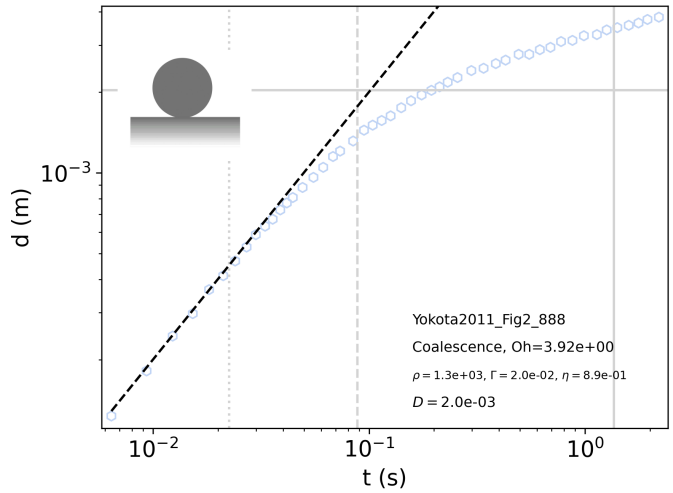

Water-glycerol mixture in PDMS oil.
A precise value of density was not available.
In a Hele-Shaw cell $D = (RH)^{\frac{1}{2}}$, where R and H are respectively the drop radius and the cell thickness.
Long-time behavior follows $d/\ell_{vc} \propto (t/\tau_{vc})^{\frac{1}{4}}$.

Paulsen2011 Fig2 1p9

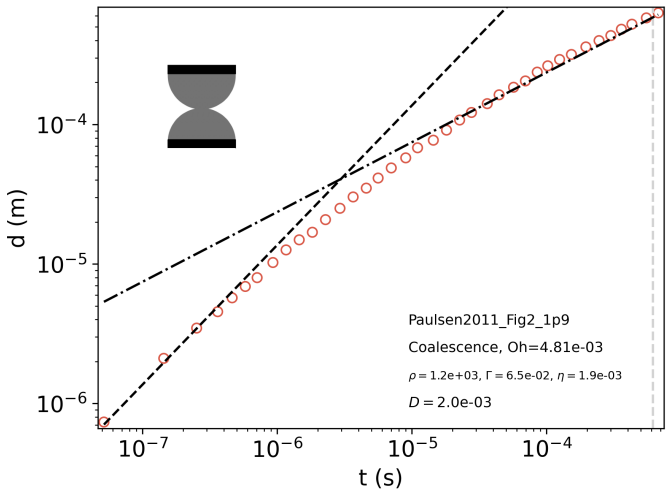

Glycerol-water-NaCl mixture in ambient air.

Paulsen2011 Fig2 11

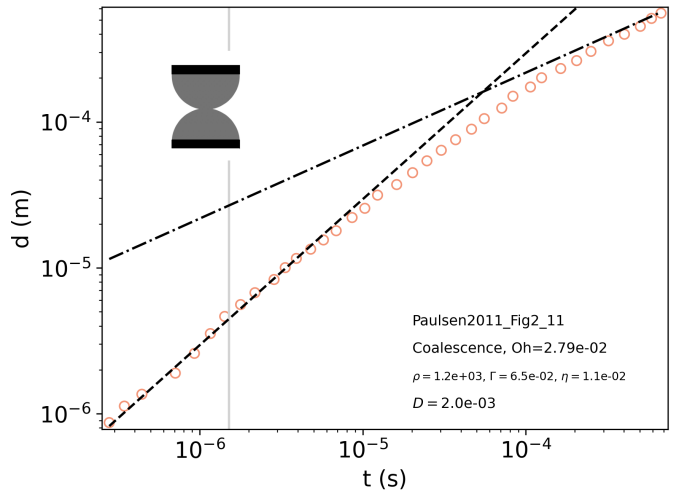

Glycerol-water-NaCl mixture in ambient air.

Paulsen2011 Fig2 48

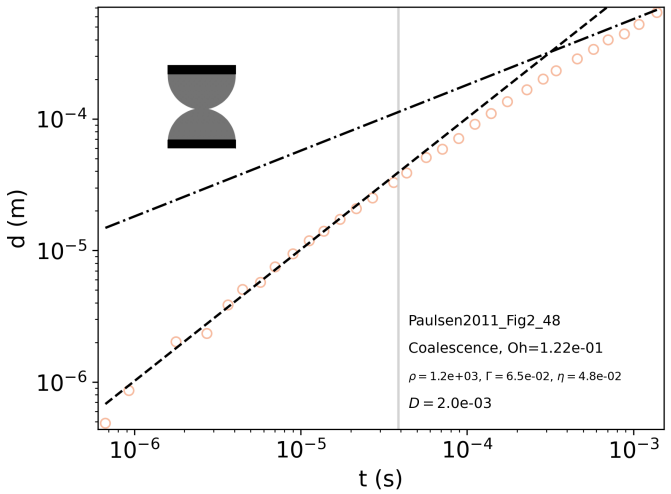

Glycerol-water-NaCl mixture in ambient air.

Paulsen2011 Fig2 230

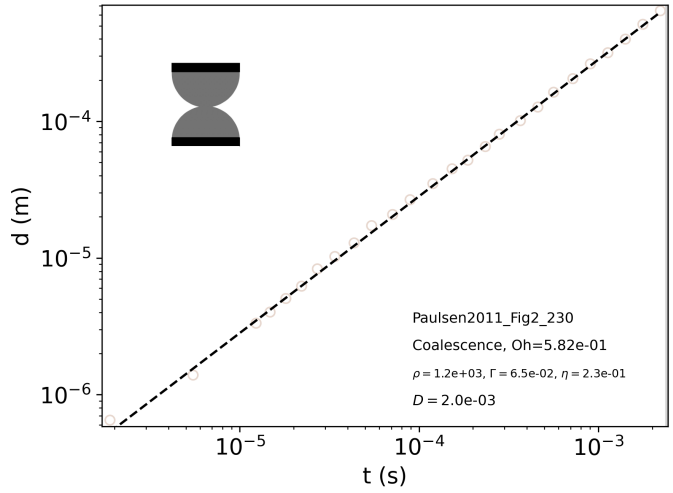

Glycerol-water-NaCl mixture in ambient air.

Paulsen2014 Fig1

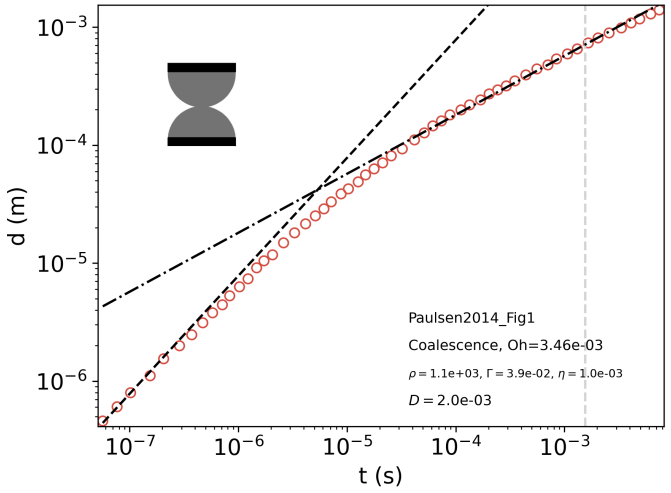

Salt water in silicone oil.

Soto2018 Fig5

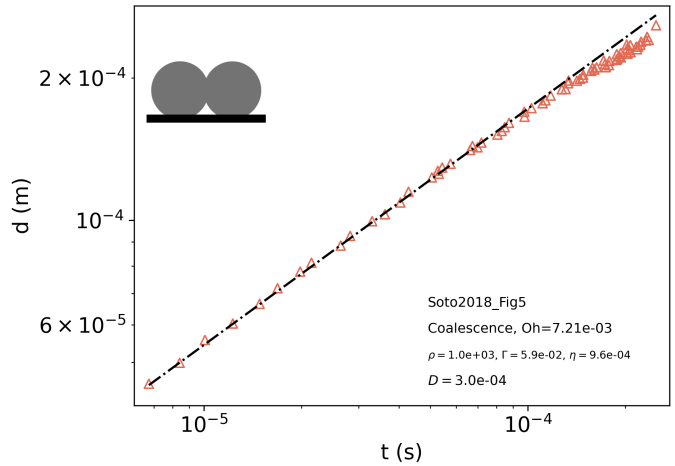

CO_2 bubble in water.
Density and viscosity are that of the outer fluid.

Rahman2019 Fig6 6p65

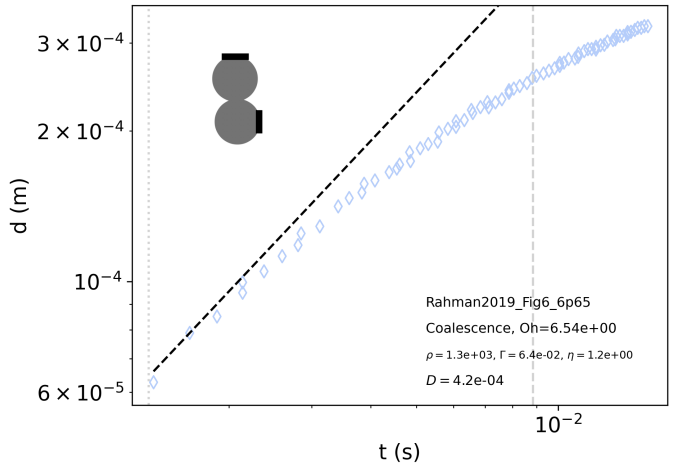

Water-glycerol mixture in ambient air.

Rahman2019 Fig6 1p84

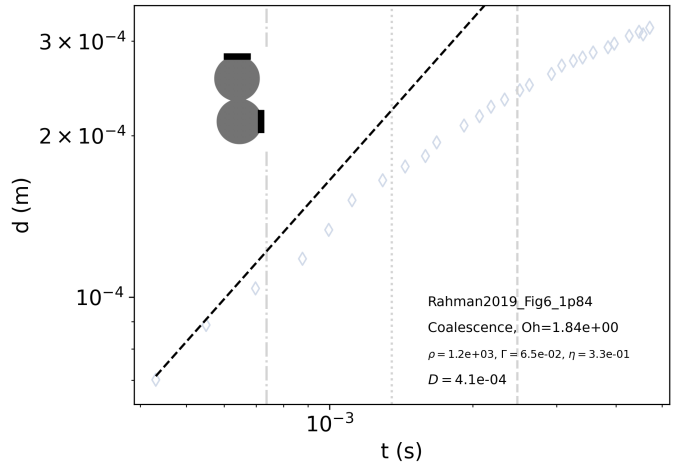

Water-glycerol mixture in ambient air.

Rahman2019 Fig6 0p146

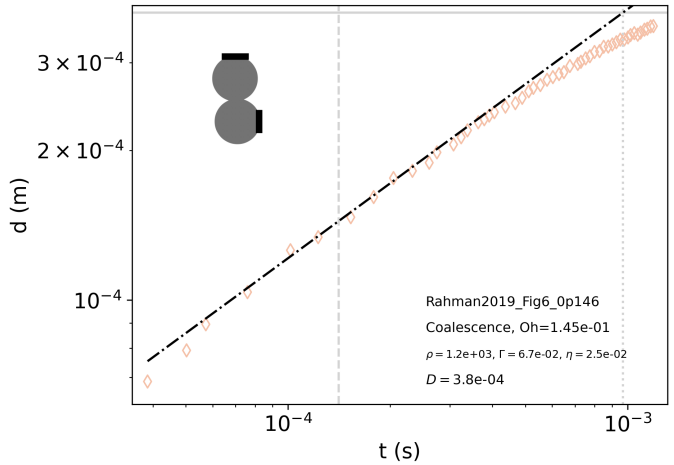

Water-glycerol mixture in ambient air.

Rahman2019 Fig6 0p00692

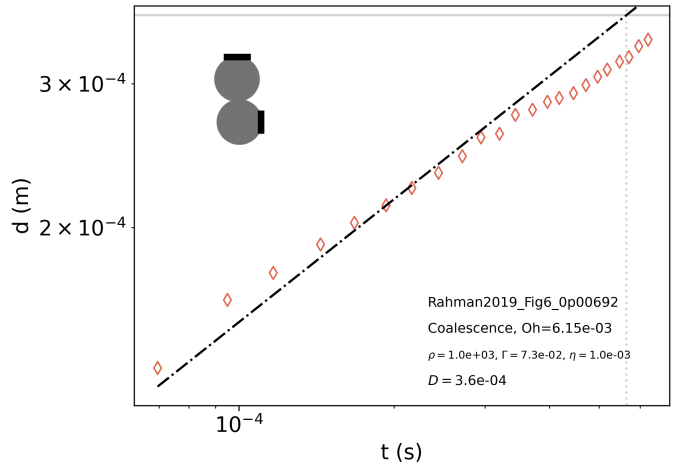

Water-glycerol mixture in ambient air.

Chen1997 Fig7

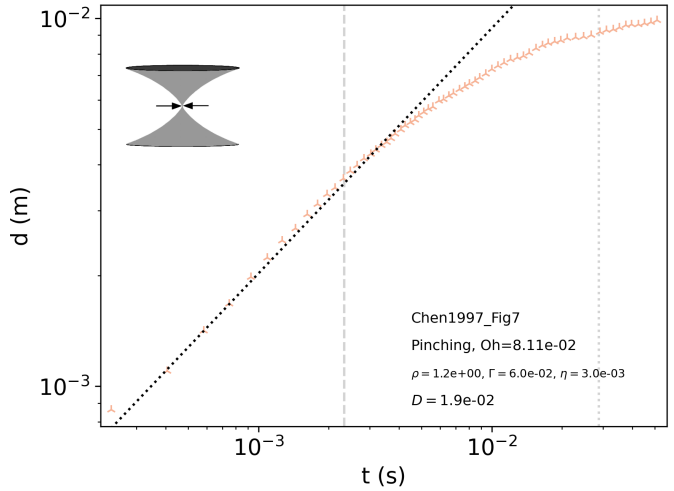

Catenoid soap film in ambient air.
Density is that of air, viscosity is that of the soap film.

McKinley2000 Fig4

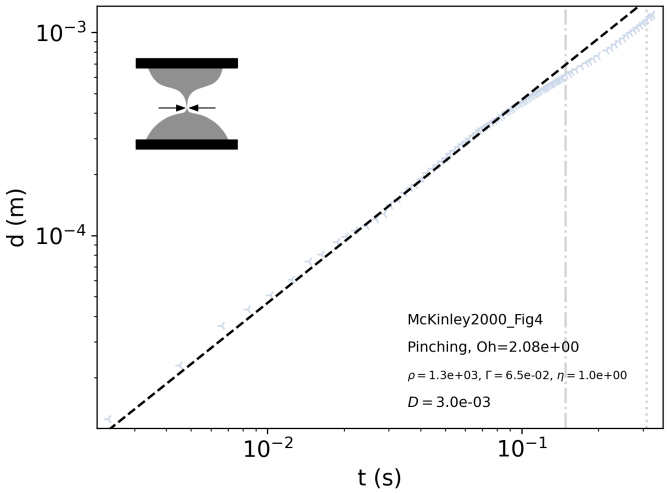

Glycerol in ambient air.

Chen2002 Fig3

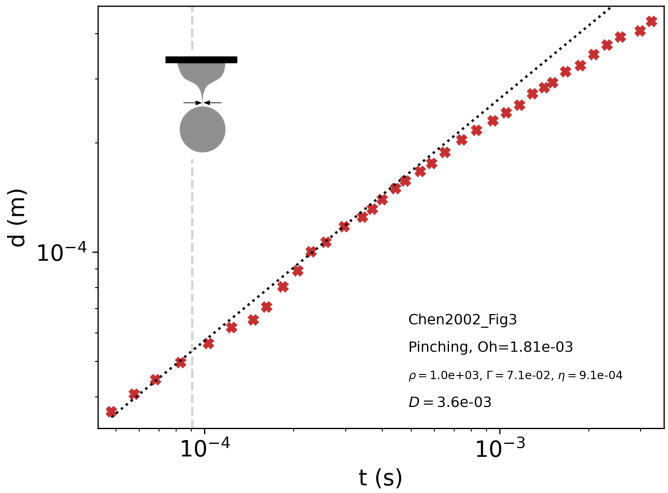

Water in ambient air.

Burton2004 Fig5

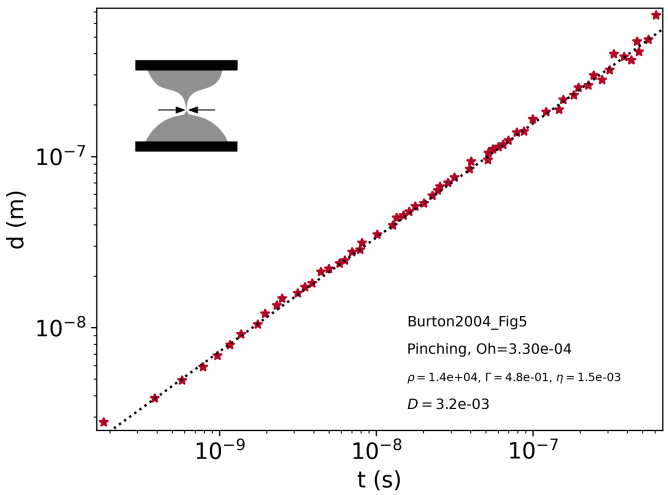

Mercury in ambient air.

Burton2005 0p9

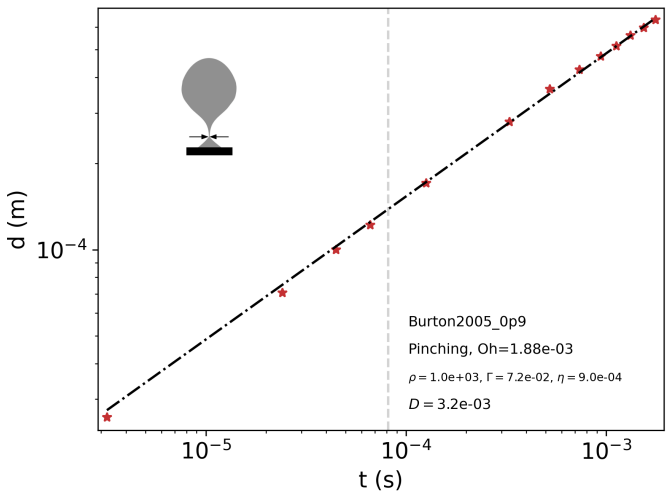

Air bubble in water.
Density and viscosity are that of the outer fluid.

Burton2005 37p4

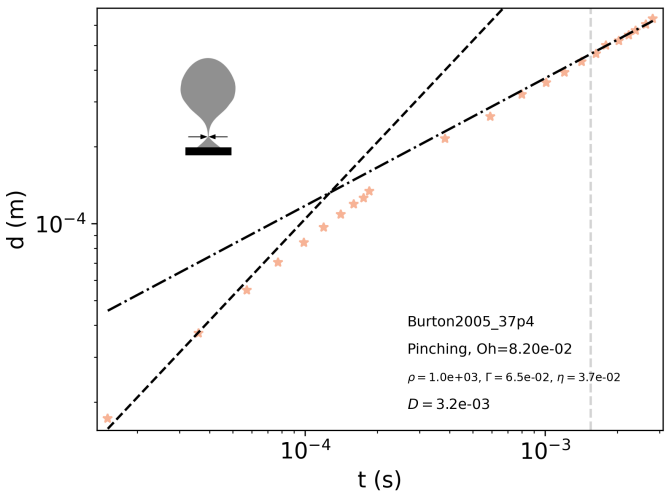

Air bubble in water-glycerol mixture.
Density and viscosity are that of the outer fluid.

Burton2005 1011

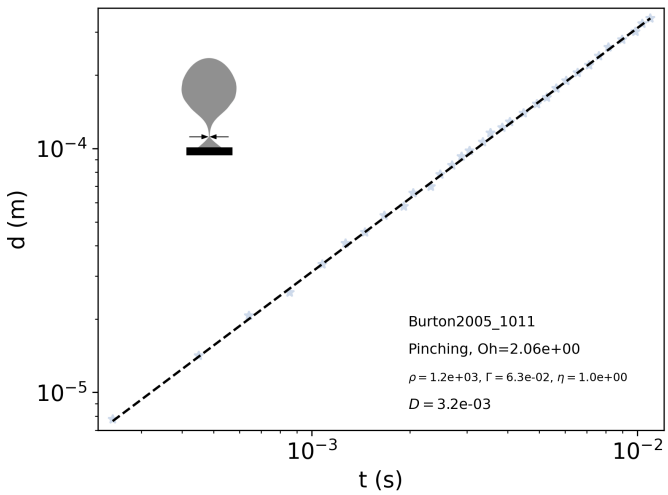

Air bubble in water-glycerol mixture.
Density and viscosity are that of the outer fluid.

Burton2007 Fig7

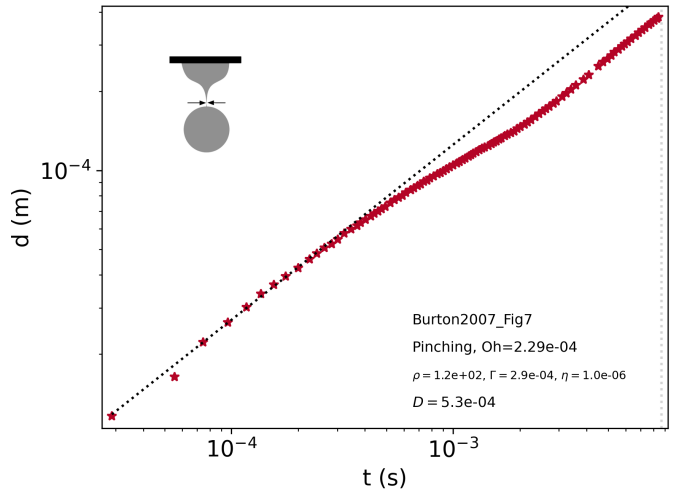

Superfluid ^{4}He at temperature T=1.34K.
No viscosity is available. The artificial value $\eta = 10^{-6}$ Pa.s is used in SI-Fig. 2b.

Keim2006 Fig2 4p1

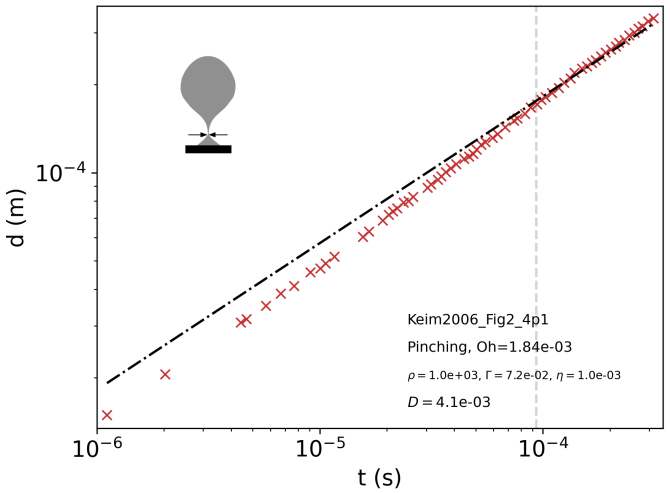

Air bubble in water.
Density and viscosity are that of the outer fluid.

Keim2006 Fig2 1p5

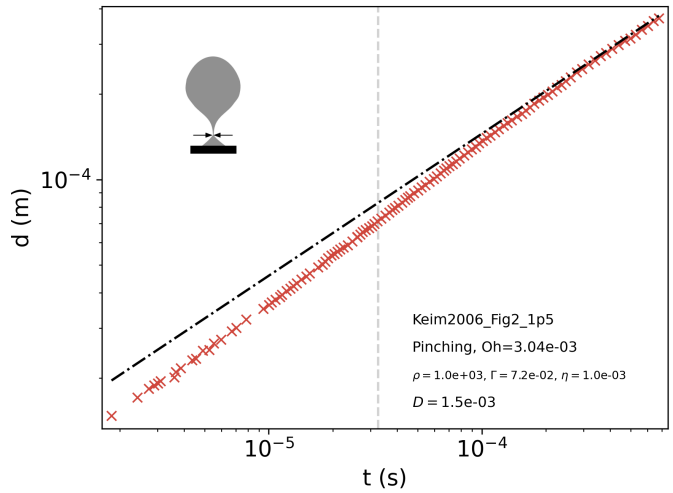

Air bubble in water.
Density and viscosity are that of the outer fluid.

Bolanos2009 Fig6 water

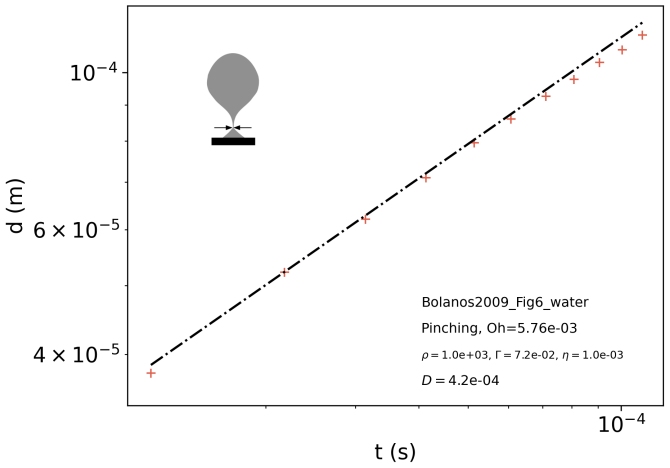

Air bubble in water.
Density and viscosity are that of the outer fluid.

Bolanos2009 Fig7 water

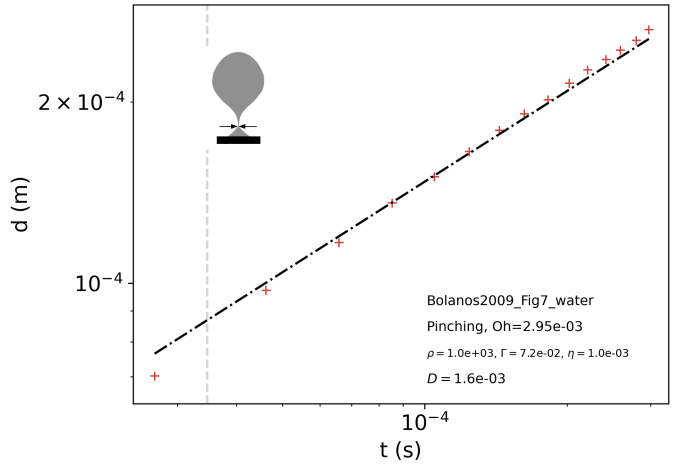

Air bubble in water.
Density and viscosity are that of the outer fluid.

Bolanos2009 Fig6 O2

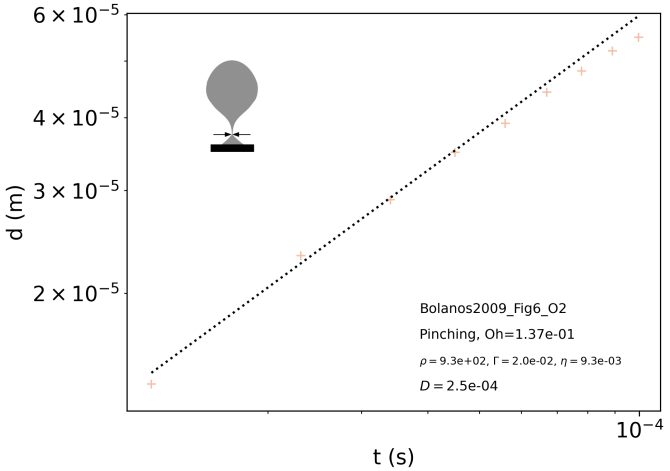

Air bubble in silicone oil.
Density and viscosity are that of the outer fluid.

Bolanos2009 Fig7 O7

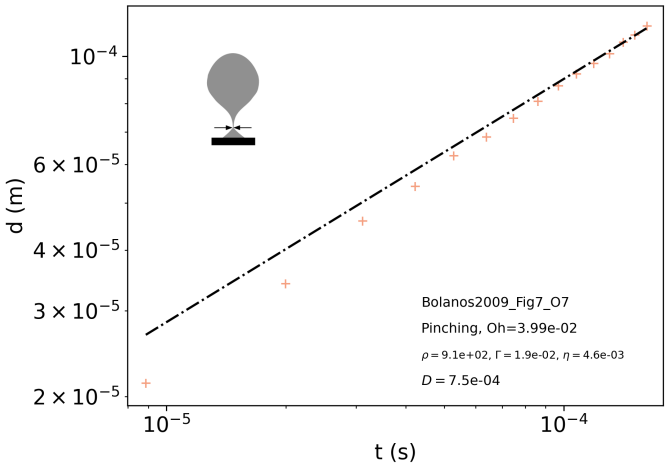

Air bubble in silicone oil.
Density and viscosity are that of the outer fluid.

Bolanos2009 Fig7 O8

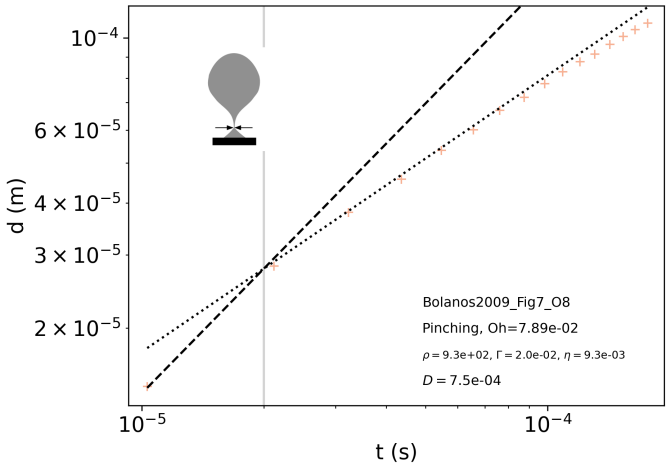

Air bubble in silicone oil.
Density and viscosity are that of the outer fluid.

Bolanos2009 Fig7 O9

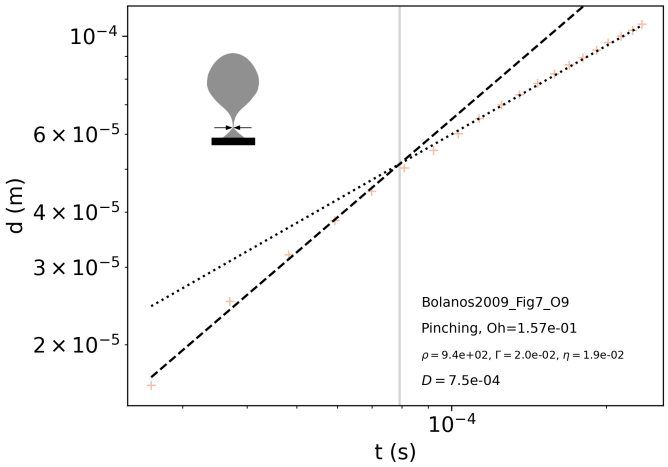

Air bubble in silicone oil.
Density and viscosity are that of the outer fluid.

Bolanos2009 Fig8 G1

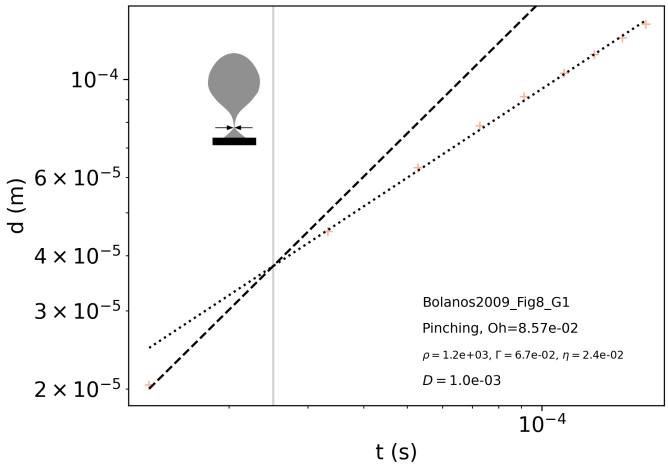

Air bubble in water-glycerol mixture.
Density and viscosity are that of the outer fluid.

Bolanos2009 Fig8 G2

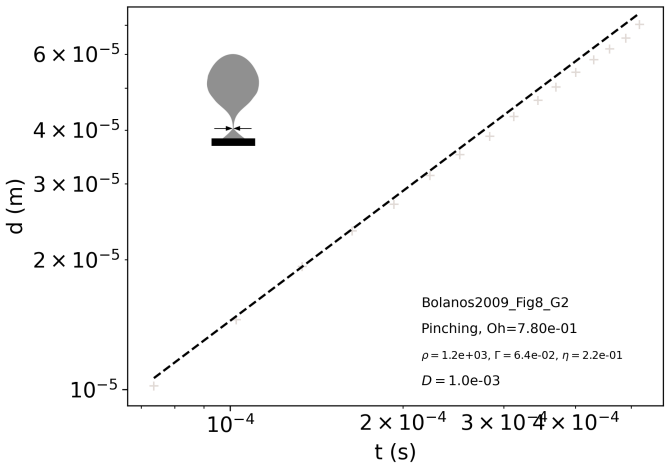

Air bubble in water-glycerol mixture.
Density and viscosity are that of the outer fluid.

Bolanos2009 Fig8 G4

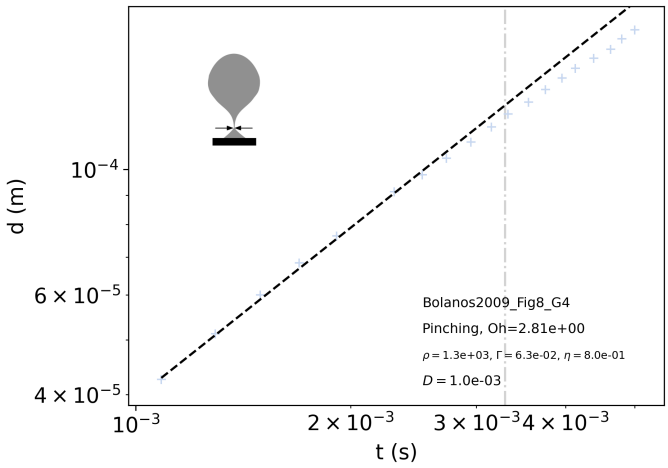

Air bubble in water-glycerol mixture.
Density and viscosity are that of the outer fluid.

Bolanos2009 Fig9 G5

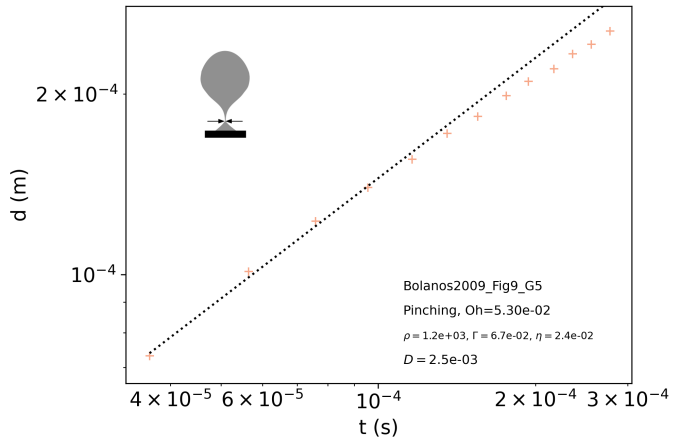

Air bubble in water-glycerol mixture.
Density and viscosity are that of the outer fluid.

Bolanos2009 Fig9 G6

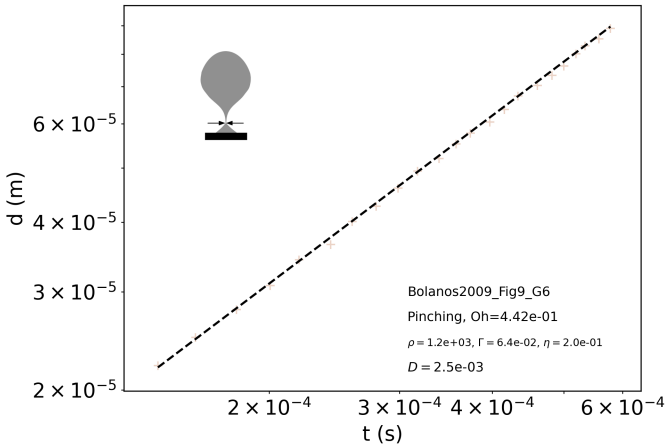

Air bubble in water-glycerol mixture.
Density and viscosity are that of the outer fluid.

Bolanos2009 Fig6 O1

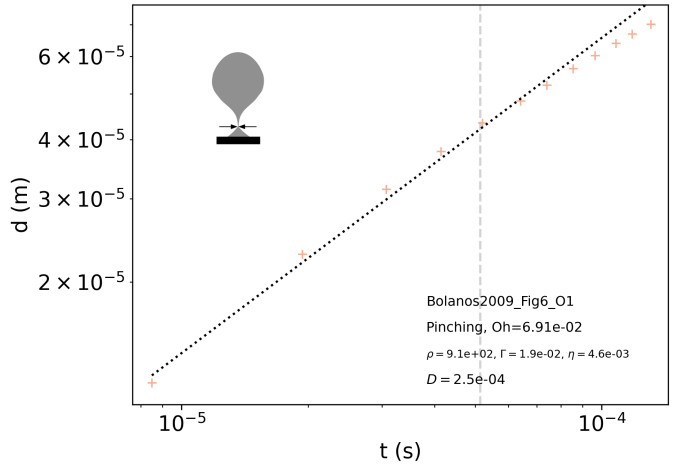

Air bubble in water-glycerol mixture.
Density and viscosity are that of the outer fluid.

Bolanos2009 Fig6 O3

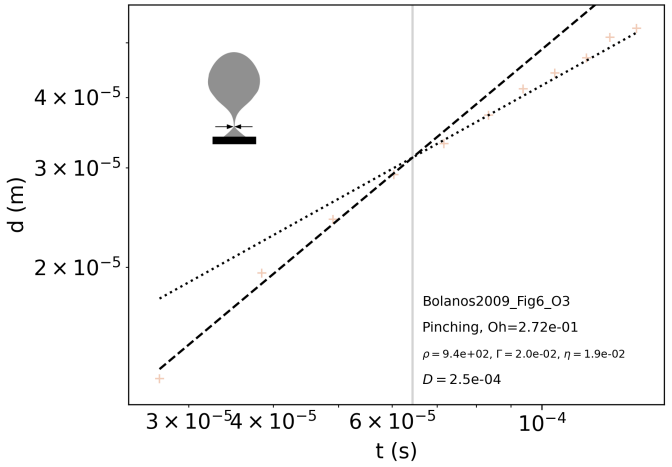

Air bubble in water-glycerol mixture.
Density and viscosity are that of the outer fluid.

Bolanos2009 Fig9 G8

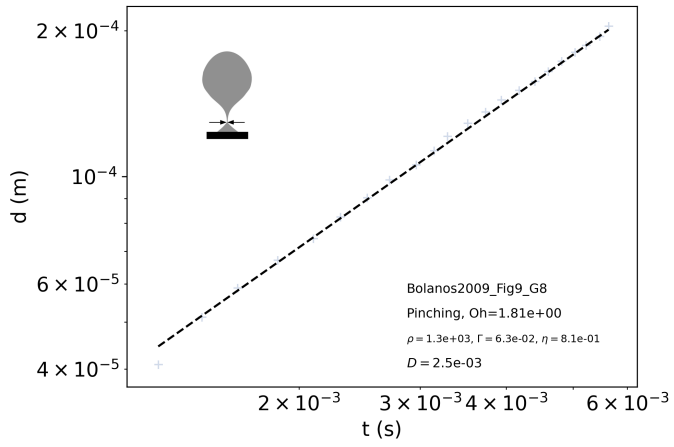

Air bubble in water-glycerol mixture.
Density and viscosity are that of the outer fluid.

Goldstein2010 Fig5

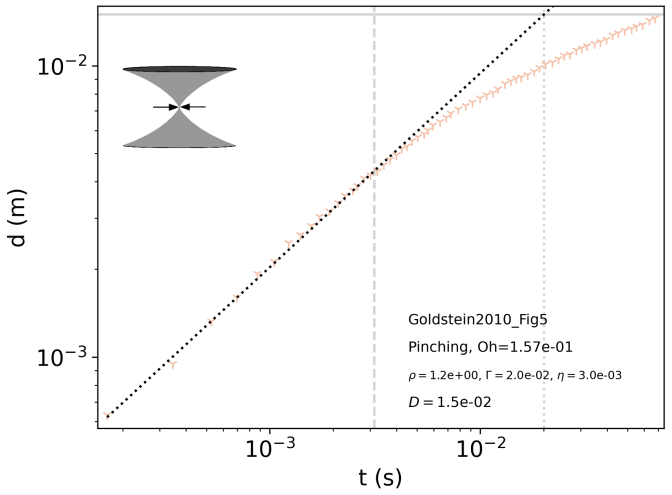

Soap film on Mobius strip.
Values of material parameters estimated since not provided.
Density is that of air, viscosity is that of soap film.

[1] J. Schindelin, I. Arganda-Carreras, E. Frise, V. Kaynig, M. Longair, T. Pietzsch, S. Preibisch, C. Rueden, S. Saalfeld, B. Schmid, et al., Nature methods **9**, 676 (2012).
[2] R. Donnelly, R. Hills, and P. Roberts, Physical Review Letters **42**, 725 (1979).
[3] E. Buckingham, Physical review **4**, 345 (1914).
[4] A. Eddi, K. G. Winkels, and J. H. Snoeijer, Physics of fluids **25**, 013102 (2013).
[5] A. Cazabat and M. C. Stuart, The Journal of Physical Chemistry **90**, 5845 (1986).
[6] A. Jaishankar and G. H. McKinley, Proceedings of the Royal Society A: Mathematical, Physical and Engineering Sciences **469**, 20120284 (2013).
[7] J. R. Castrejón-Pita, A. A. Castrejón-Pita, S. S. Thete, K. Sambath, I. M. Hutchings, J. Hinch, J. R. Lister, and O. A. Basaran, Proceedings of the National Academy of Sciences **112**, 4582 (2015).